

University of New Hampshire

University of New Hampshire Scholars' Repository

Master's Theses and Capstones

Student Scholarship

Spring 2021

Warming temperatures increase microbial consumption of marine organic matter

Sarah Benson

University of New Hampshire, Durham

Follow this and additional works at: <https://scholars.unh.edu/thesis>

Recommended Citation

Benson, Sarah, "Warming temperatures increase microbial consumption of marine organic matter" (2021). *Master's Theses and Capstones*. 1448. <https://scholars.unh.edu/thesis/1448>

This Thesis is brought to you for free and open access by the Student Scholarship at University of New Hampshire Scholars' Repository. It has been accepted for inclusion in Master's Theses and Capstones by an authorized administrator of University of New Hampshire Scholars' Repository. For more information, please contact Scholarly.Communication@unh.edu.

**WARMING TEMPERATURES INCREASE MICROBIAL CONSUMPTION OF
MARINE ORGANIC MATTER**

by

SARAH M. BENSON

B.S. Biology, University of Wisconsin – Whitewater, 2017

THESIS

Submitted to the University of New Hampshire
in Partial Fulfilment of
the Requirements for the Degree of

Master of Science

In

Oceanography

May, 2021

This thesis was examined and approved in partial fulfillment of the requirements for the degree of Master of Science in Oceanography by:

Dr. Robert Letscher
Thesis Director
Assistant Professor in Earth Sciences and
Assistant Director of Ocean Process Analysis
Laboratory

Dr. Kai Ziervogel
Research Associate Professor and
Director of Ocean Process Analysis Laboratory

Dr. Elizabeth Harvey
Assistant Professor in Biological Sciences

On April 8th, 2021

Approval signatures are on file with the University of New Hampshire Graduate School.

TABLE OF CONTENTS

ACKNOWLEDGEMENTS	iv
LIST OF FIGURES	v
LIST OF TABLES	vii
ABSTRACT	viii

	PAGE
INTRODUCTION	1
METHODS	5
RESULTS	10
2019 Experiment	10
2020 Experiment	18
2019 to 2020 Experiment Comparison	30
Q ₁₀	33
DISCUSSION	33
REFERENCES	40

ACKNOWLEDGEMENTS

First and foremost, I would like to express my deepest and most sincere gratitude to my advisor Dr. Robert Letscher and for the opportunity he gave me to conduct research under his mentorship. He has provided endless support, patience, guidance, motivation, and excitement during my M.S. coursework, research, and composition of this thesis. I could not have asked for a better advisor and mentor for the last two years at the University of New Hampshire.

In addition to my advisor, I would also like to thank the other members of my committee, Dr. Kai Ziervogel and Dr. Elizabeth Harvey, who have been encouraging and provided insightful feedback throughout this process. I also appreciate them teaching me new laboratory and statistical procedures, and for allowing me to use their laboratories for sample filtering and analysis.

A special thanks to the crew of the R/V Gulf Challenger for taking me out to my collection locations and to the UNH Water Quality Lab for processing particulate organic carbon and nitrogen filters.

Finally, I would like to thank my friends and family for their continuous love and support.

LIST OF FIGURES

Figure 1: Collection sites in the Gulf of Maine for 2019 and 2020 experiment.

Figure 2: NASA OceanColor Web Satellite chlorophyll α concentrations for (a) 2019 seawater collection on October 14, 2019 and (b) 2020 seawater collection on October 3, 2020.

Figure 3: Experimental set up and measurements taken from each triplicate.

Figure 4: Carbon concentrations for F, FI, and FIPOM. Error bars for (a): ± 0.81 (14°) and ± 0.99 (19°), (b): ± 1.09 , (c): ± 1.12 , (d): ± 1.36 , and (e): ± 1.32 .

Figure 5: Nitrogen concentrations for F, FI, and FIPOM. Error bars for (a): ± 0.015 (14°) and ± 0.022 (19°), (b): ± 0.038 , (c): ± 0.033 , (d): ± 0.062 , and (e): ± 0.062 .

Figure 6: Nitrate concentrations for F, FI, and FIPOM. Error bars (a): ± 0.11 (14°) and ± 0.025 (19°), (b): ± 0.025 , (c): ± 0.014 , (d): ± 0.058 , and (e): ± 0.048 .

Figure 7: Phosphate concentrations for F, FI, and FIPOM. Error bars (a): ± 0.043 (14°) and ± 0.05 (19°), (b): ± 0.036 , (c): ± 0.032 , (d): ± 0.032 , and (e): ± 0.037 .

Figure 8: C:N ratios determined from POC and PON pool. N:P ratios determined from dissolved nitrate and phosphate pools. Error bars for (a): $\pm 6.4\%$, (b): $\pm 4.4\%$, (c): $\pm 6.4\%$ (d): $\pm 4.4\%$, (e): $\pm 6.4\%$, and (f): $\pm 4.4\%$.

Figure 9: Particles/mL for F and FIPOM in each incubation. Error bars (a): ± 1.6 , (b): ± 2.11 , (c): ± 5.16 , and (d): ± 6.94 .

Figure 10: Average particle area (μm^2) for F and FIPOM incubations. Note F axes are not the same as the FIPOM axes. Error bars (a): ± 110.74 , (b): ± 141.41 , (c): ± 39.45 , and (d): ± 41.35 .

Figure 11: Cell counts/mL ($\times 10^5$) for F and FIPOM in each incubation. Error bars (a): ± 0.587 , (b): ± 0.553 , (c): ± 0.353 , and (d): ± 0.173 .

Figure 12: Carbon concentrations for F and FIPOM. Event One ($T_0 - T_2$) and Event Two ($T_8 - T_{14}$) illustrated in FIPOM. Error bars for (a) ± 0.75 (12°) and ± 0.91 for 18, (b): ± 0.87 , and (c): ± 0.79 .

Figure 13: Nitrogen concentrations for F and FIPOM. Error bars for (a): ± 0.011 (12°) and ± 0.01 (18°), (b): ± 0.021 , and (c): ± 0.019 .

Figure 14: Phosphorus concentrations for F and FIPOM. Error bars for (a): ± 0.003 (12°) and ± 0.003 (18°), (b): ± 0.002 , and (c): ± 0.01 .

Figure 15: Nitrate concentrations for F and FIPOM. Error bars for (a): ± 0.002 (12°) and ± 0.002 (18°), (b): ± 0.021 , and (c): ± 0.013 .

Figure 16: Phosphate concentrations for F and FIPOM. Error bars for (a): ± 0.012 (12°) and ± 0.016 (18°), (b): ± 0.024 , and (c): ± 0.031 .

Figure 17: C:N:P ratios using POC, PON, and POP pools. Note the y – axis for F - C:N and F - C:P are not the same as FIPOM - C:N and FIPOM - C:P axes. Error bars for (a): $\pm 6.4\%$, (b): $\pm 4.4\%$, (c): $\pm 5.3\%$, (d): $\pm 6.4\%$, (e): $\pm 4.4\%$, and (f): $\pm 5.3\%$.

Figure 18: a. FIPOM - C 2019 rates versus 2020 rates. b. FIPOM - C 2019 deltas versus 2020 deltas. Error bars for (a) is the uncertainty in the fit: ± 0.273 (12°), ± 0.209 (14°), ± 0.322 (18°), and ± 0.02 (19°), and (b) is $\pm 5\%$ of the delta from analytical uncertainty.

Figure 19: a. FIPOM - N 2019 rates versus 2020 rates. b. FIPOM - N 2019 deltas versus 2020 deltas. Error bars for (a) is the uncertainty in the fit: ± 0.008 (12°), ± 0.018 (14°), ± 0.008 (18°), and ± 0.034 (19°), and (b) is $\pm 4\%$ of the delta from analytical uncertainty.

Figure 20: a. FIPOM - NO_3^- 2019 rates versus 2020 rates. b. FIPOM - NO_3^- 2019 deltas versus 2020 deltas. Error bars for (a) is the uncertainty in the fit: ± 0.005 (12°), ± 0.012 (14°), ± 0.004 (18°), and ± 0.013 (19°), and (b) is $\pm 4\%$ of the delta from analytical uncertainty.

Figure 21: a. FIPOM - PO_4^{3-} 2019 rates versus 2020 rates. b. FIPOM - PO_4^{3-} 2019 deltas versus 2020 deltas. Error bars for (a) is the uncertainty in the fit: ± 0.012 (12°), ± 0.001 (14°), ± 0.013 (18°), and ± 0.003 (19°), and (b) is $\pm 2\%$ of the delta from analytical uncertainty.

LIST OF TABLES

Table 1: Sample Nomenclature

Table 2: Rate and uncertainty ($\mu\text{M}/\text{day}$), delta (Δ ; μM), t – test to determine if rate is significantly different than 0 with a 95% confidence level ($p < 0.05$), and ANOVA p – value for the 2019 experiment concentrations from $T_0 - T_8$ with a 95% confidence level ($p < 0.05$). Bolded p – values are significantly different.

Table 3: FlowCAM pictures of particles from T_2 and T_{14} for F and FIPOM treatments at both incubation temperatures.

Table 4: Rate and uncertainty ($\mu\text{M}/\text{day}$), delta (Δ ; μM), t – test to determine if rate is significantly different than 0 with a 95% confidence level ($p < 0.05$), and ANOVA p – value for the 2020 experiment concentrations from $T_0 - T_{14}$ with a 95% confidence level ($p < 0.05$). Bolded p – values are significantly different.

Table 5: Analysis of covariance determined if the rate of consumption/production in the experimental temperature incubation is significantly different than the rate of consumption/production in the in situ temperature incubation for the FIPOM elemental pools ($p < 0.05$).

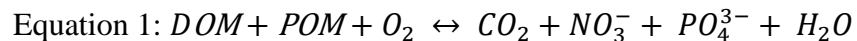
Table 6: Q_{10} calculations for the FIPOM elemental pool for 2019 and 2020, with 2020 events (POC) and delays (PON and POP).

ABSTRACT

Marine microbes are vital to oceanic ecosystems and influence the global climate through their paramount role in Earth's biogeochemical cycles. With this intricate role in ecosystems, it is important to understand the effect of increasing ocean temperatures on the cycling of organic matter (OM), which is hypothesized to contribute a positive feedback to future warming via an acceleration in microbial respiration of OM to CO₂. We experimentally investigated the temperature sensitivity of microbial consumption of marine particulate OM focused in the rapidly warming Gulf of Maine during the 2019 and 2020 Fall phytoplankton bloom. The overall rate and quantity of microbial OM (C, N, and P pools) consumption at in situ versus elevated temperatures were quantified within bottle incubations over the course of two weeks. The results indicate that OM incubated at warmer temperatures (+5 – 6°C) was consumed at a faster rate with an overall larger quantity consumed compared to cooler temperatures (12 – 14°C). Additionally, nitrate that initially accumulated from the consumption of particulate organic nitrogen (PON), was readily consumed at later time points at both temperatures, possibly related to the carbon-rich, nitrogen-poor quality of the in situ OM. In 2020, more nitrogen-rich OM was preferentially consumed at cooler temperatures, leaving behind carbon-rich OM. Whereas at warmer temperatures, carbon-rich OM was preferentially consumed presumably due to it being a bioavailable energy source to fuel elevated metabolic rates. The empirically estimated temperature coefficient (Q_{10}) ranged from 2.66 – 3.42 in 2019 versus 0.94 – 1.21 in 2020, dependent on the OM elemental pool, suggesting temperature plays an important role in OM consumption, but is not the only factor contributing to the rates and magnitude of OM consumption by marine microbes.

INTRODUCTION

In a single drop of seawater, hundreds of thousands of microbes are thriving. Marine microbes are fundamental to ecosystems as they recycle organic matter (OM), which is composed primarily of detritus, and provide essential nutrients to other organisms. Through microbial respiration, dissolved organic matter (DOM) and particulate organic matter (POM) are consumed along with oxygen and regenerated into bioavailable nutrients (e.g., CO_2 , NO_3^- , PO_4^{3-}) (Alldredge & Silver, 1988; Equation 1). Photosynthesis and respiration rates are highest during a phytoplankton bloom and are important to the productivity and biodiversity of a region; contributing to the biological carbon pump (BCP) where atmospheric CO_2 is absorbed and sequestered in the deep ocean. In the Gulf of Maine, there are two phytoplankton blooms: Spring and Fall (Thomas et al., 2003). Following wintertime ocean mixing, more nutrients are available for phytoplankton, causing a larger bloom in Spring and creating more OM in comparison to Fall. In addition to more nutrients, there is an increase in sunlight, which is needed to catalyze photosynthesis (Gran & Braarud, 1935; Townsend & Spinrad, 1986; Durbin et al., 2003). During Fall, an increase in storms with water temperatures decreasing from cooling air temperatures creates a deeper mixed layer depth introducing nutrients to the surface ocean, fueling a phytoplankton bloom (Sigler et al., 2014).



During a phytoplankton bloom with an effective BCP, more OM is being produced than respired resulting in high biological productivity and should have an elemental composition close to the Redfield ratio of 106 C: 16 N: 1 P (Redfield, 1934; Redfield, 1958). When the Redfield ratio was determined, it was set as a global standard and not individually based on the productivity in different latitudinal regions. However, more recently POM found at 40°N had a mean

stoichiometric composition of 198 C: 27 N: 1 P, where the C:N (7.3 : 1) is greater than the Redfield 6.6 C: 1 N (Martiny et al., 2013). Overall, Martiny et al. (2013) found a global average of OM C:P and N:P stoichiometry that was 23 – 38% greater than the standard Redfield ratio depending on the latitude, primarily driven by temperature, available nutrients, and biological diversity. Heterotrophic microbes favor nutrient rich OM such as particulate organic nitrogen (PON) and particulate organic phosphorus (POP) and leave behind particulate organic carbon (POC) rich OM (Zweifel et al., 1993; Schneider et al., 2003). Marine microbes are crucial for recycling blooms and regenerating the nutrients necessary to sustain them, while at the same time contribute to the sequestration of carbon in the deep ocean to be preserved for millennia. Thus, the potential impacts on these organisms and their metabolisms due to climate change could have consequences to marine ecosystems.

Morán et al. (2018) identified increased temperatures as part of seasonal variability led to a faster growth rate of marine microbes. In addition, both increasing substrate concentrations and temperatures approaching the thermal optimum growth temperature, have been found to significantly reduce generation time (Pomeroy and Wiebe, 2001). Rapid growth rates at warmer temperatures may be related to faster enzymatic rates which catalyze metabolic reactions by lowering the activation energy (E_a). The E_a does not change with temperature but is related to the temperature through the Arrhenius Law Equation (Equation 2), with a larger E_a translating to a larger temperature sensitivity for a given reaction. Warming temperatures are also thought to have an impact on microbial community composition and have been shown to cause shifts in individual adaptations to be able to survive in changing conditions (Yvon-Durocher et al., 2016; Trombetta et al., 2019).

$$\text{Equation 2: } K_c = A \cdot e^{-E_a/R \cdot T}$$

Temperature is known to influence many metabolic rates in nature, comprising a key tenet of the metabolic theory of ecology (Brown et al., 2004). The sensitivity of metabolic rates to temperature is most often expressed using the temperature coefficient (Q_{10}), which relates the fractional change in a rate for an increase of 10°C . Many biological reactions have a Q_{10} near 2, meaning with an increase of 10°C , the reaction rate will double. For example, respiration of soil OM is estimated to exhibit a mean Q_{10} of ~ 2 with important regional variability between 1 (no temperature stimulation) to maximal values of ~ 2.6 (Zhou et al., 2009). However, this sensitivity for microbial respiration of marine DOM and POM is relatively unknown in the ocean. From the standard metabolic theory of ecology, photosynthesis and respiration rates should increase as temperatures increase which were later verified by Regaudie-de-Gioux and Duarte in 2012. From their study, the empirically estimated E_a was higher for respiration than for photosynthesis, yielding the prediction that microbial OM consumption may outpace primary production in a warming ocean. Additionally, Rivkin and Legendre (2001) reported a 2.5% decrease in bacterial growth efficiency (BGE) for every increase of 1°C , which contradicts the Pomeroy and Wiebe (2001) prediction of enhanced growth rates, as bacteria allocate more carbon to respiration than to biomass with the increase in temperature. In 2018, Lønborg et al. determined the Q_{10} of marine dissolved organic carbon (DOC) in the global oceans ranging from 1.7 – 1.8 and 4 – 8, with the composition of DOC (labile, semi-labile, semi-refractory, and refractory) being a major factor. Brewer and Peltzer (2017) illustrated how marine respiration rates at different depths will respond to temperature changes differently, as oxygen consumption is driven by temperature not depth, as it is related to the Arrhenius Law Equation. An increase in oxygen consumption with increasing temperatures could potentially lead to more hypoxic regions in the ocean to develop. In addition to hypoxic regions, increasing microbial respiration has the potential to create larger areas of CO_2

outgassing, weakening the ocean CO₂ sink, and further contributing to climate change (López-Urrutia et al., 2006).

The Gulf of Maine in the mid-latitude NW Atlantic Ocean has been warming 99% faster than the global oceans, since 2012, thought to result from a northward shift in the position of the Gulf Stream, cutting off cool waters within the Labrador Current flowing south around the Canadian Maritime provinces to fill into the basin (Rossby and Benway, 2000; Pershing et al., 2015). As marine microbes respire OM back into bioavailable nutrients at a more rapid rate, the amount of nutrients getting to the seafloor communities would be reduced (e.g., benthic lobsters) and less carbon would be sequestered. It is clear the sensitivity of marine microbial consumption of OM to temperature warrants further study. A focus on the rapidly warming Gulf of Maine may serve as a ‘canary in the coal mine’ for the expected ecological and biogeochemical consequences of ocean warming for both coastal and open ocean ecosystems alike. The present study sought to answer three questions related to the temperature sensitivity of microbial consumption of marine OM, tested with waters collected following the Fall phytoplankton bloom in the Gulf of Maine in 2019 and 2020. (1) Do experimentally warmer water temperatures correlate to a faster rate of OM consumption by the in situ microbial community? (2) Do these warmer temperatures correlate to an overall larger amount of OM respired compared to the cooler in situ temperature? (3) What is the Q₁₀ of OM consumption in the Gulf of Maine? These questions were addressed by using bottle incubation experiments in two temperature-controlled rooms for a duration of 8 – 14 days whereby the microbial consumption of OM, regeneration of inorganic nutrients, and growth of bacterial cells were followed.

METHODS

Study Site

Seawater collection sites for the 2019 and 2020 incubation experiment were in the Gulf of Maine, north of Appledore Island, off the coast of New Hampshire at 2m below the surface through an intake hose underneath the R/V Gulf Challenger and collected into

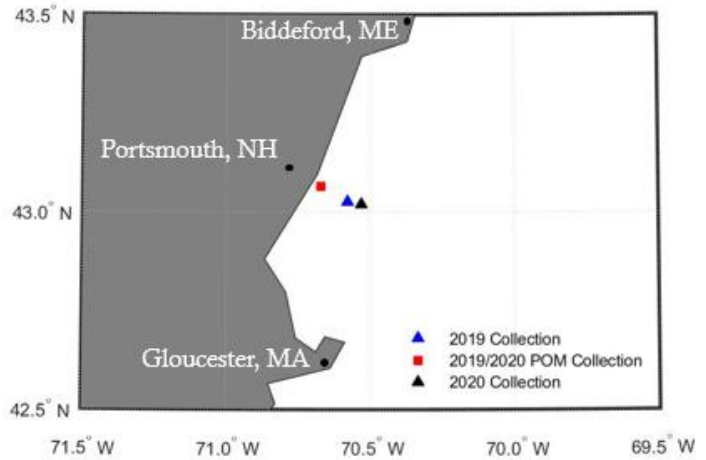


Figure 1: Collection sites in the Gulf of Maine for 2019 and 2020 experiment.

20L polypropylene carboys (43.013° N,

70.345° W and 43.011° N, 70.316° W, for 2019 and 2020, respectively, Figure 1). Coastal seawater from 43.036° N, 70.402° W was collected for additional POM to be added to the experimental incubations due to the larger amount of substrate from coastal influence.

Experiment

Bulk seawater was collected in October during the Fall 2019 phytoplankton bloom and in October 2020 prior to the Fall bloom (Figure 2). Chlorophyll α concentrations measured from satellites are used as a proxy for primary production (i.e., phytoplankton bloom). Sixty L of collected seawater was filtered using a 0.2- μ m capsule filter to remove all POM and biomass with

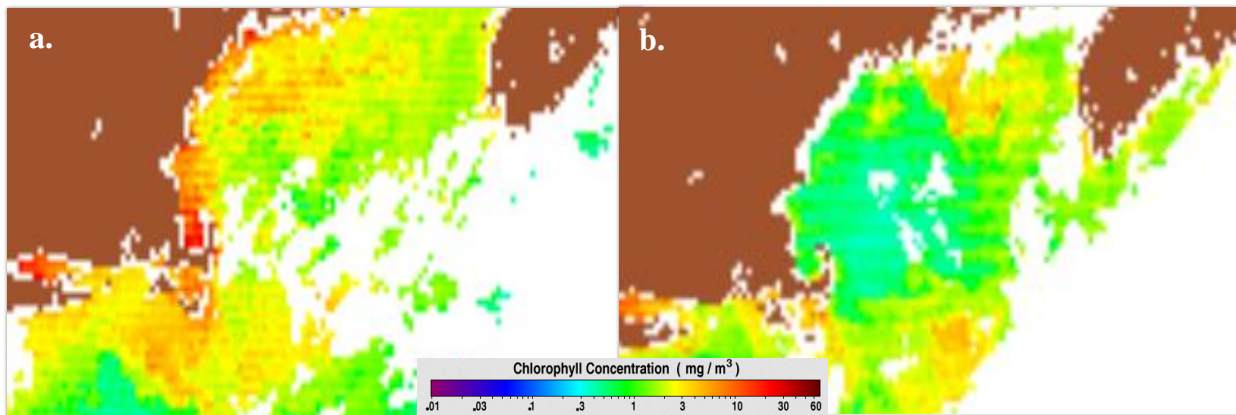


Figure 2: NASA OceanColor Web Satellite chlorophyll α concentrations for (a) 2019 seawater collection on October 14, 2019 and (b) 2020 seawater collection on October 3, 2020.

20 L left as whole seawater to be used as the inoculum, containing both the in situ microbial community and POM. Ten L of coastal seawater was filtered using a pre-combusted (4 hours at 450°C) 47mm 0.7- μm glass fiber filter (GFF) to collect additional POM to be added to the experiment by scraping off the particles and mixed into the water. Seawater and POM was allocated into three treatments: 100% 0.2- μm Filtered (F), 80% Filtered + 20% Inoculum (FI), and 80% Filtered + 20% Inoculum + POM (FIPOM). An 80/20 mixture was used to release marine microbes from grazing pressure, allowing exponential growth to occur and rapid consumption of substrate. Treatments were put into one-liter pre-combusted glass Pyrex media bottles, placed on a roller table to prevent particles from settling, and in a dark, temperature-controlled incubation room to inhibit photosynthesis.

For the 2019 experiment, four F, twelve FI, and twelve FIPOM bottles were randomly placed in the 14°C incubation (in situ) or the 19°C incubation (+5°C experimental) room, for a total of 28 bottles incubated for 8 days in both incubation rooms. To obtain the initial incubation seawater conditions, one F, FI, and FIPOM bottle were randomly selected. Ten mL were set aside for cell counts¹ with one mL added to a 2 mL cryovial pre-loaded with 0.255 mL of 1% paraformaldehyde and 0.01% glutaraldehyde fixative and stored in liquid nitrogen (-196°C, Kamiya et al., 2007). Additionally, 250 mL of each individual bottle were filtered through a 25mm 0.2- μm polycarbonate filter to collect DNA¹ and placed in liquid nitrogen (-196°C). Three hundred fifty mL from individual bottles were vacuum filtered through a pre-combusted 25mm 0.7- μm GFF to collect POM for analysis of particulate organic carbon (POC) and particulate organic nitrogen (PON) content. The filtrate was collected in acid-washed 60 mL HDPE bottles for dissolved organic carbon (DOC)¹, nitrate + nitrite ($\text{NO}_3^- + \text{NO}_2^-$, hereafter NO_3^-), and phosphate

¹ Collected samples not processed due to COVID – 19 shutdown.

(PO_4^{3-}) analysis. At each time point [T = 2, 4, 6, 8 days], one F, three FI, and three FIPOM were randomly selected from each incubation chamber to be filtered. FI and FIPOM bottles were assigned A, B, and C. GFFs and nutrient bottles were placed at -20°C for analysis after incubation termination.

For the 2020 experiment, the FI treatment was eliminated to focus on POM and to allow for a longer duration of the experiment given space constraints on the roller tables. Seven F and twenty-one FIPOM bottles were randomly placed in the 12°C incubation (in situ) or the 18°C incubation ($+6^\circ\text{C}$ experimental), for a total of 28 bottles incubated for 14 days in both incubation chambers. Initial (T = 0) seawater conditions were collected as in 2019. At each time point [T = 2, 4, 6, 8, 10, 12, 14 days], one F and three FIPOM bottles were randomly selected from each incubation chamber. FIPOM bottles were assigned A, B, and C. POC, PON, DOC^1 , NO_3^- , PO_4^{3-} , and cell counts were collected the same as 2019. In addition, 50mL of water was set aside to quantify the number and average area of particles per mL through a flow imaging microscope (FlowCAM) to capture high-resolution images of particles between 12 and $300\text{-}\mu\text{m}$ from three analysis runs of 10 mL of the sample to determine if particles were decreasing in numbers and area through the duration of the incubation. Additionally, in 2020, filters for the analysis of particulate organic phosphorus (POP) were collected through the same method as POC and PON. DNA^1 was collected from 100mL of each bottle filtering through the same filter size as 2019. See Figure 3 for experimental set up.

Analytical Methods

Nitrate was analyzed by chemiluminescence following reduction to $\text{NO}_{(\text{gas})}$ with a vanadium (III) solution using the method from Braman and Hendrix (1989), with an analytical

¹ Collected samples not processed due to COVID – 19 shutdown.

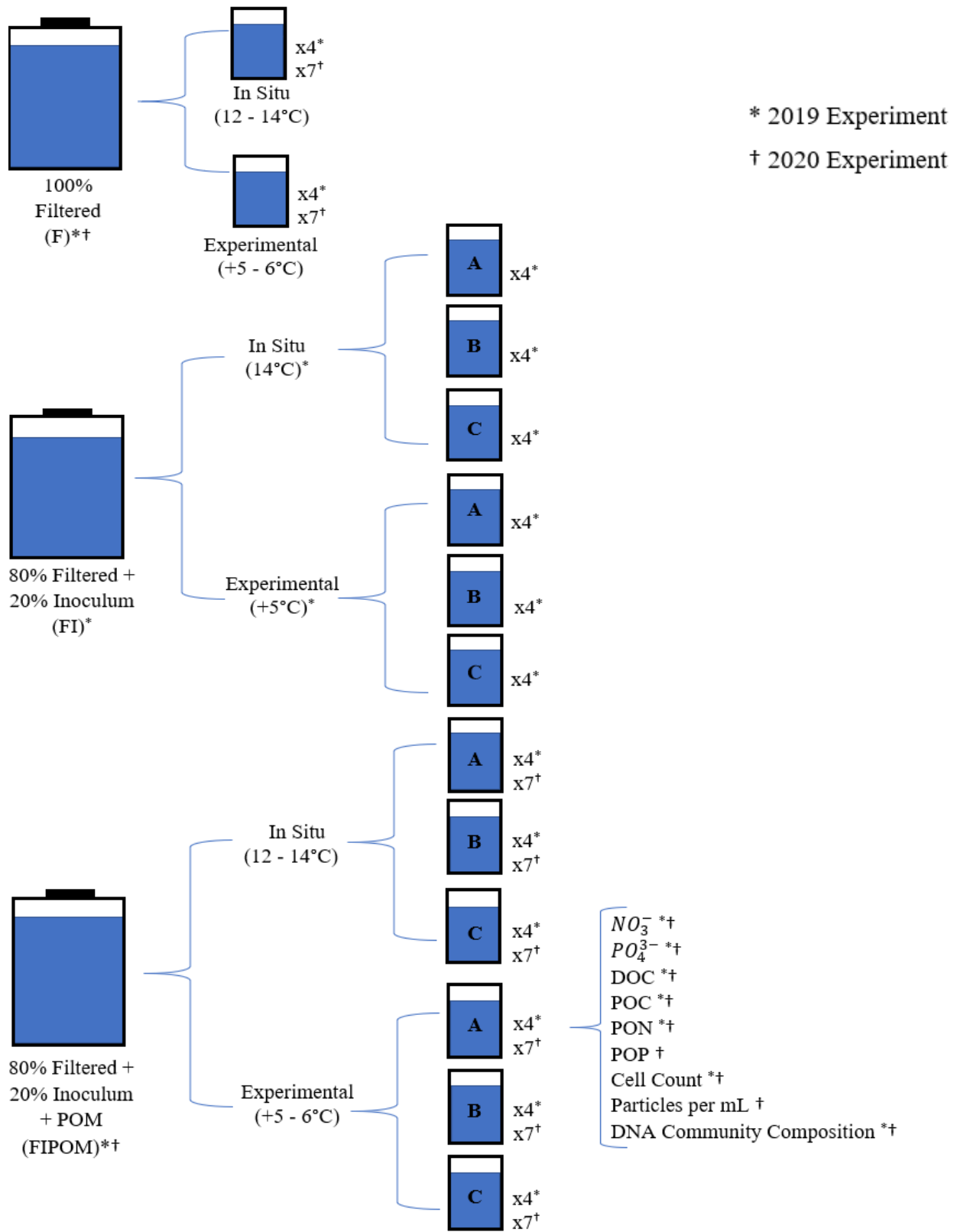


Figure 3: Experimental set up and measurements taken from each triplicate.

uncertainty of 4% and limit of detection (LOD) of 0.01 μM . Phosphate was analyzed using a modified version of the molybdenum blue spectrophotometry method from Strickland and Parsons (1968) using a 10 cm pathlength and a 885 nm wavelength, with an analytical uncertainty of 2% and LOD of 0.025 μM . POP was analyzed using a modified version of the ash hydrolysis method from Solórzano and Sharp (1980) to oxidize all organic P to PO_4^{3-} followed by quantification using the same modified spectrophotometry method from Strickland and Parsons (1968), with an analytical uncertainty of 2% and LOD of 0.025 μM . POC and PON was analyzed by the UNH Water Quality Lab by combustion with CHN elemental analysis, with an analytical uncertainty of 5% and 4% with a LOD of 0.4 μM , respectively. Cell counts were analyzed by flow cytometry after staining with SYBR Green following Kamiya et al. (2007). Particles were analyzed using a 4x objective lens with a FlowCAM.

Data Analysis

All data analysis was conducted in MATLAB[®]. Property versus time point plots were created for each experimentally monitored parameter with time point equal to days since incubation initiation ($T = 0$). The overall difference (delta, Δ) in the concentration from T_0 to T_{Final} was calculated to determine the total quantity of OM consumed or nutrient produced, dependent on the elemental pool. To understand the relationship between temperature and OM consumption, and between temperature and nutrient production, a trend line was fitted to the data using linear regression for each treatment to obtain a rate per day ($\mu\text{M}/\text{day}$). Two parameters were used to prevent overfitting. Uncertainty in the fit was calculated from the residuals of the trend line and a t – test was completed on the rate to determine if it was significantly different than 0, using a confidence level of 95% ($p < 0.05$). ANOVA Two – Factor without Replication was used to determine if the measured concentrations over the duration of the experiment ($T_0 - T_{\text{Final}}$) of an elemental pool for each treatment and temperature was significantly different from one another

(e.g., Concentrations of FIPOM – C 12 ($T_0 - T_{14}$) versus concentrations of FIPOM – C 18 ($T_0 - T_{14}$.) Analysis of covariance was calculated based on the slope and uncertainty from the linear regression for the respected elemental OM pool for both the 2019 and 2020 experiment, to determine if the rate of consumption or production in the warmer temperature incubation was significantly different than the rate of consumption or production in the cooler temperature incubation.

Q_{10}

Based on the rates obtained from the linear regression trend line, the Q_{10} was calculated using the equation from Kirschbaum (1995; Equation 3) where R_1 and R_2 are the rates obtained from the fit of the line. T_1 is the cooler temperature and T_2 is the warmer temperature for each experiment.

$$\text{Equation 3: } Q_{10} = \left(\frac{R_2}{R_1} \right)^{\left(\frac{10}{T_2 - T_1} \right)}$$

RESULTS

Nomenclature

Samples are identified by the treatment, elemental pool, and the incubation temperature (Table 1).

Table 1: Sample Nomenclature.

Treatment	Treatment Acronym	Elemental Pool	Temperature (°C)
100% Filtered	F	Carbon (C)	12
80% Filtered + 20% Inoculum	FI	Nitrogen (N)	14
80% Filtered + 20% Inoculum + POM	FIPOM	Phosphorus (P)	18
		Nitrate (NO_3^-)	19
		Phosphate (PO_4^{3-})	

2019 Experiment

Table 2 summarizes results from the 2019 experiment, presenting for $T_0 - T_8$: rates and uncertainty ($\mu\text{M}/\text{day}$), overall difference from T_8 to T_0 in concentration to determine net consumption or production (Δ ; μM), t – test calculated from the slope of the linear regression

and uncertainty to determine if the rate was significantly different than 0 ($p < 0.05$), and the statistical significance from ANOVA Two – Factor without Replication if the measured concentrations of an elemental pool for each treatment was significantly different from one another ($p < 0.05$).

Table 2: Rate and uncertainty ($\mu\text{M}/\text{day}$), delta (Δ ; μM), t – test to determine if rate is significantly different than 0 with a 95% confidence level ($p < 0.05$), and ANOVA p – value for the 2019 experiment concentrations from $T_0 - T_8$ with a 95% confidence level ($p < 0.05$). Bolded p – values are significantly different.

Sample ID	Rate ($\mu\text{M}/\text{day}$) \pm Uncertainty in Rate ($\mu\text{M}/\text{day}$)	Delta (Δ ; μM)	t – test p – value of rate	ANOVA [In situ] vs [Experimental] p - value
F – C 14	-0.512 ± 0.142	-3.96	0.11	0.723
F – C 19	0.973 ± 0.568	9.77	0.11	
FI – C 14	-0.166 ± 0.175	-1.07	0.22	0.392
FI – C 19	-0.806 ± 0.314	-4.31	0.06	
FIPOM – C 14	-0.547 ± 0.209	-6.04	0.06	0.066
FIPOM – C 19	-0.893 ± 0.02	-6.77	0.005	
F – N 14	0.019 ± 0.019	0.051	0.21	0.254
F – N 19	0.064 ± 0.021	0.579	0.23	
FI – N 14	0.001 ± 0.016	0.018	0.47	0.328
FI – N 19	-0.081 ± 0.045	-0.361	0.11	
FIPOM – N 14	-0.050 ± 0.018	-0.461	0.05	0.078
FIPOM – N 19	-0.092 ± 0.034	-0.566	0.06	
F – NO_3^- 14	-0.034 ± 0.025	-0.116	0.15	0.483
F – NO_3^- 19	-0.004 ± 0.007	-0.058	0.30	
FI – NO_3^- 14	-0.024 ± 0.009	-0.189	0.06	0.011
FI – NO_3^- 19	-0.031 ± 0.006	-0.246	0.01	
FIPOM – NO_3^- 14	-0.022 ± 0.012	-0.111	0.10	0.213
FIPOM – NO_3^- 19	-0.007 ± 0.013	-0.00057	0.33	
F – PO_4^{3-} 14	-0.001 ± 0.002	0.009	0.40	0.61
F – PO_4^{3-} 19	0.009 ± 0.000	0.040	0.18	
FI – PO_4^{3-} 14	-0.003 ± 0.002	-0.018	0.14	0.042
FI – PO_4^{3-} 19	-0.002 ± 0.002	-0.025	0.24	
FIPOM – PO_4^{3-} 14	0.006 ± 0.001	0.044	0.02	0.049
FIPOM – PO_4^{3-} 19	0.011 ± 0.003	0.095	0.03	

Carbon

Figure 4 illustrates the changes in the POC elemental pool from $T_0 - T_8$ for the F, FI, and FIPOM treatments at both incubation temperatures. In the F - C treatment, the cooler incubation has an overall net consumption ($-0.512 \pm 0.142 \mu\text{M}/\text{day}$, $\Delta = -3.96 \mu\text{M}$), with the warmer incubation having an overall net production of carbon ($0.973 \pm 0.568 \mu\text{M}/\text{day}$, $\Delta = 9.77 \mu\text{M}$). Whereas in the FI - C treatments for both incubation temperatures, have overall net consumption, ($-0.166 \pm 0.175 \mu\text{M}/\text{day}$, $\Delta = -1.07 \mu\text{M}$ (14°); $-0.806 \pm 0.314 \mu\text{M}/\text{day}$, $\Delta = -4.31 \mu\text{M}$ (19°)), with the warmer incubation temperature having a faster consumption rate and larger delta in comparison to the cooler incubation temperature. Additionally, the FIPOM - C treatments for both incubation

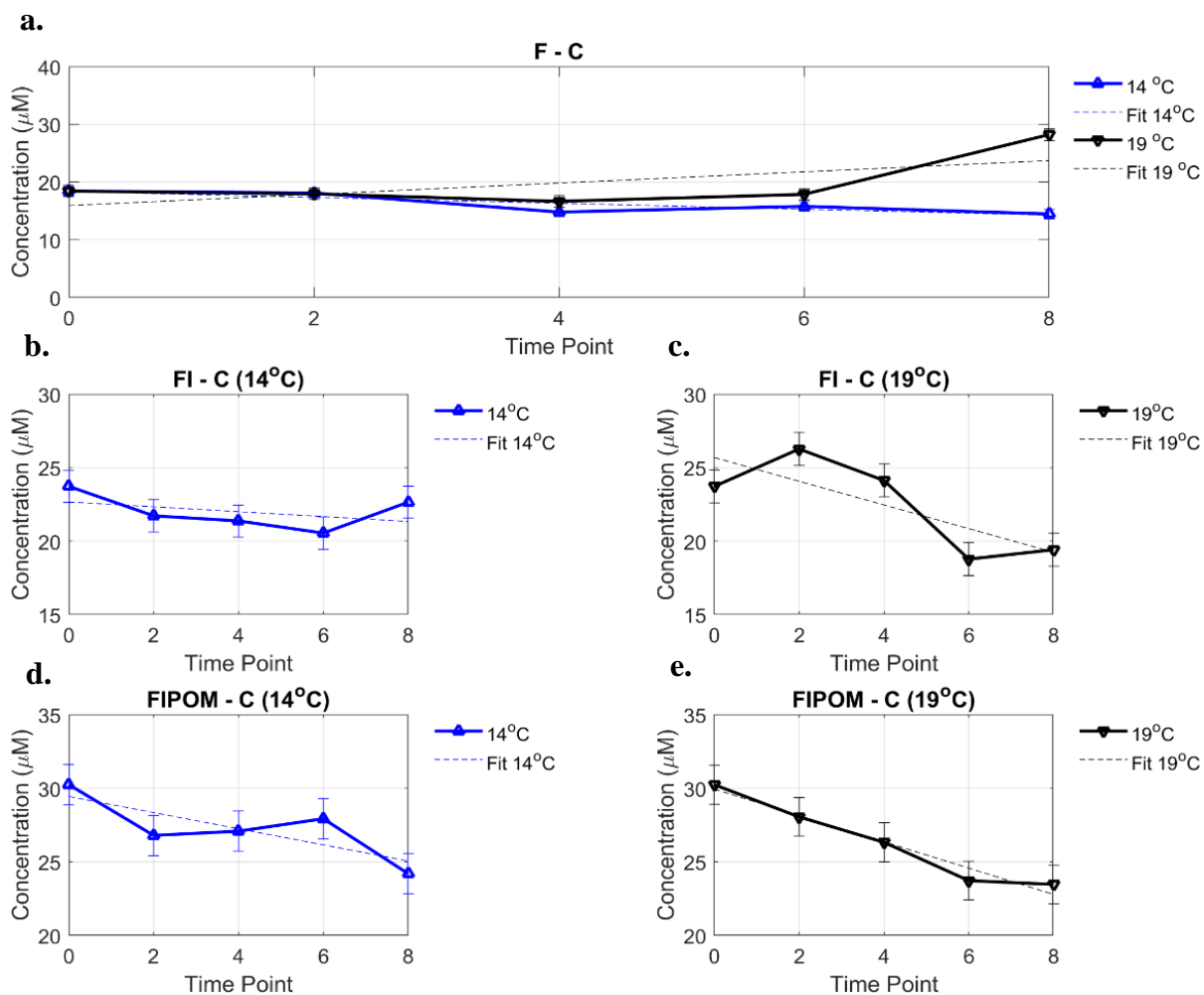


Figure 4: Carbon concentrations for F, FI, and FIPOM. Error bars for (a): ± 0.81 (14°) and ± 0.99 (19°), (b): ± 1.09 , (c): ± 1.12 , (d): ± 1.36 , and (e): ± 1.32 .

temperatures have overall net consumption ($-0.547 \pm 0.209 \mu\text{M}/\text{day}$, $\Delta = -6.04 \mu\text{M}$ (14°); and $-0.893 \pm 0.02 \mu\text{M}/\text{day}$, $\Delta = -6.77 \mu\text{M}$ (19°)), with the warmer incubation temperature having a faster consumption rate and larger delta in comparison to the cooler incubation temperature. FIPOM – C 14 and FIPOM – C 19 concentrations over the duration of the experiment have a 93.4% chance of being different from one another ($p = 0.066$).

Nitrogen

Figure 5 illustrates the changes in the PON pool from $T_0 - T_8$ for the F, FI, and FIPOM treatments at both incubation temperatures. Both temperatures in the F – N treatment had an overall net production of PON ($0.019 \pm 0.019 \mu\text{M}/\text{day}$, $\Delta = 0.051 \mu\text{M}$ (14°); and $0.064 \pm 0.021 \mu\text{M}/\text{day}$, $\Delta = 0.579 \mu\text{M}$ (19°)), with a faster production rate and larger delta in the warmer incubation

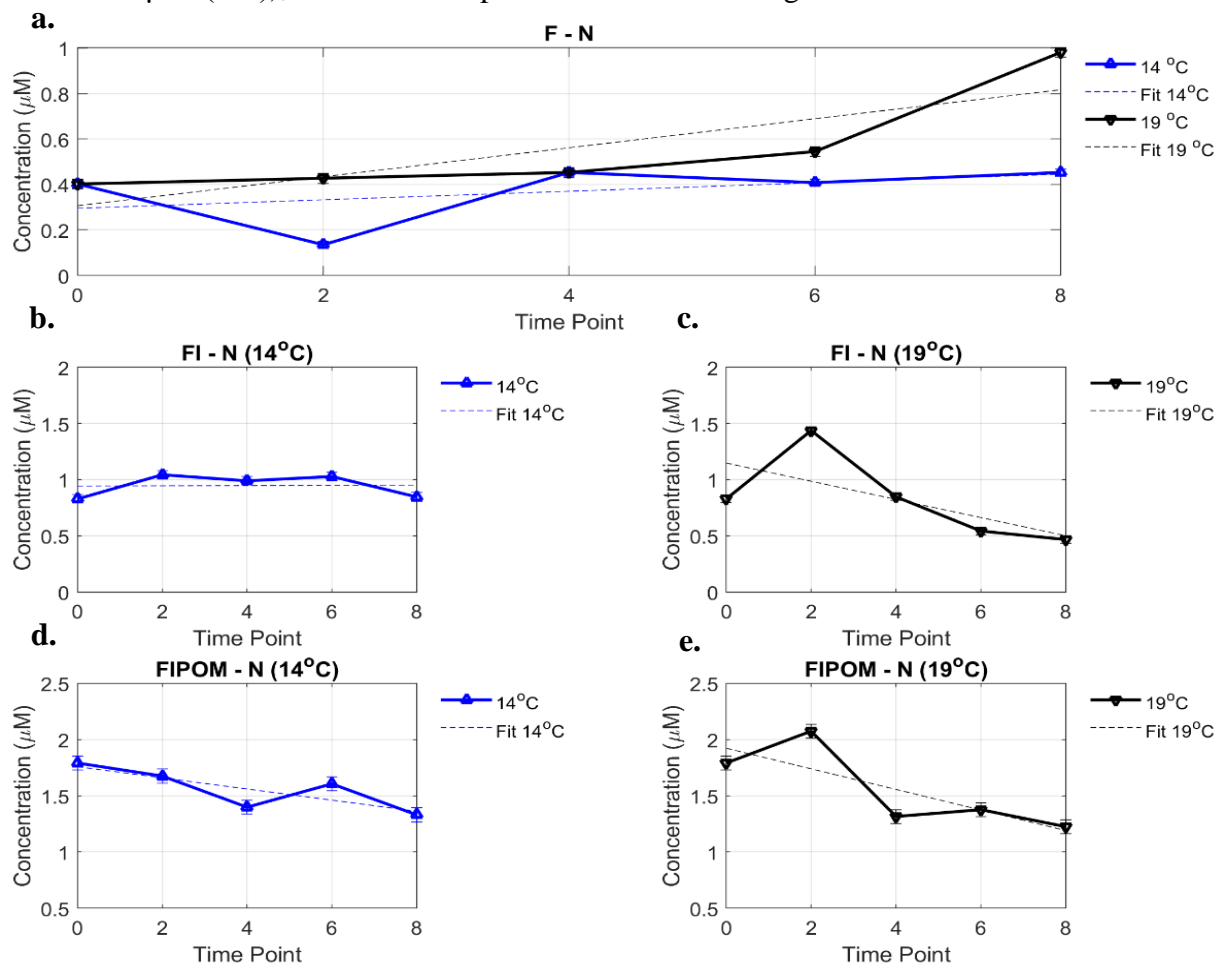


Figure 5: Nitrogen concentrations for F, FI, and FIPOM. Error bars for (a): ± 0.015 (14°) and ± 0.022 (19°), (b): ± 0.038 , (c): ± 0.033 , (d): ± 0.062 , and (e): ± 0.062 .

treatment. The cooler temperature incubation of the FI – N treatment had an overall net production of PON ($0.001 \pm 0.016 \mu\text{M}/\text{day}$, $\Delta = 0.018 \mu\text{M}$), whereas the warmer temperature incubation had an overall net consumption of PON ($-0.081 \pm 0.045 \mu\text{M}/\text{day}$, $\Delta = -0.361 \mu\text{M}$). For FIPOM – N, both temperatures had an overall net PON consumption ($-0.050 \pm 0.018 \mu\text{M}/\text{day}$, $\Delta = -0.461 (14^\circ)$; and $-0.092 \pm 0.034 \mu\text{M}/\text{day}$, $\Delta = -0.566 \mu\text{M} (19^\circ)$). Similar to the carbon elemental pool, faster rates and larger deltas were observed in the warmer temperature incubation for the FIPOM treatment. Additionally, FIPOM – N 14 and FIPOM – N 19 concentrations over the duration of the experiment have a 92.2% chance of being different from one another ($p = 0.078$).

Nitrate

Over the course of the experiment, the F, FI, and FIPOM treatments at both temperature incubations had an overall net consumption of NO_3^- (Figure 6). FI – NO_3^- had faster consumption rates and larger deltas in the warmer temperature incubation ($-0.031 \pm 0.006 \mu\text{M}/\text{day}$, $\Delta = -0.246 \mu\text{M}$) compared to the cooler temperature incubation ($-0.024 \pm 0.009 \mu\text{M}/\text{day}$, $\Delta = -0.189 \mu\text{M}$). Whereas F – NO_3^- and FIPOM – NO_3^- had faster consumption rates and larger deltas in the cooler temperature incubation ($-0.034 \pm 0.025 \mu\text{M}/\text{day}$, $\Delta = -0.016 \mu\text{M}$ (F); and $-0.022 \pm 0.012 \mu\text{M}/\text{day}$, $\Delta = -0.111 \mu\text{M}$ (FIPOM)) in comparison to the warmer temperature incubation ($-0.004 \pm 0.007 \mu\text{M}/\text{day}$, $\Delta = -0.058 \mu\text{M}$ (F); and $-0.007 \pm 0.013 \mu\text{M}/\text{day}$, $\Delta = -0.00057 \mu\text{M}$ (FIPOM)). FI – NO_3^- 14 and FI – NO_3^- 19 concentrations over the duration of the experiment were significantly different from one another ($p = 0.011$).

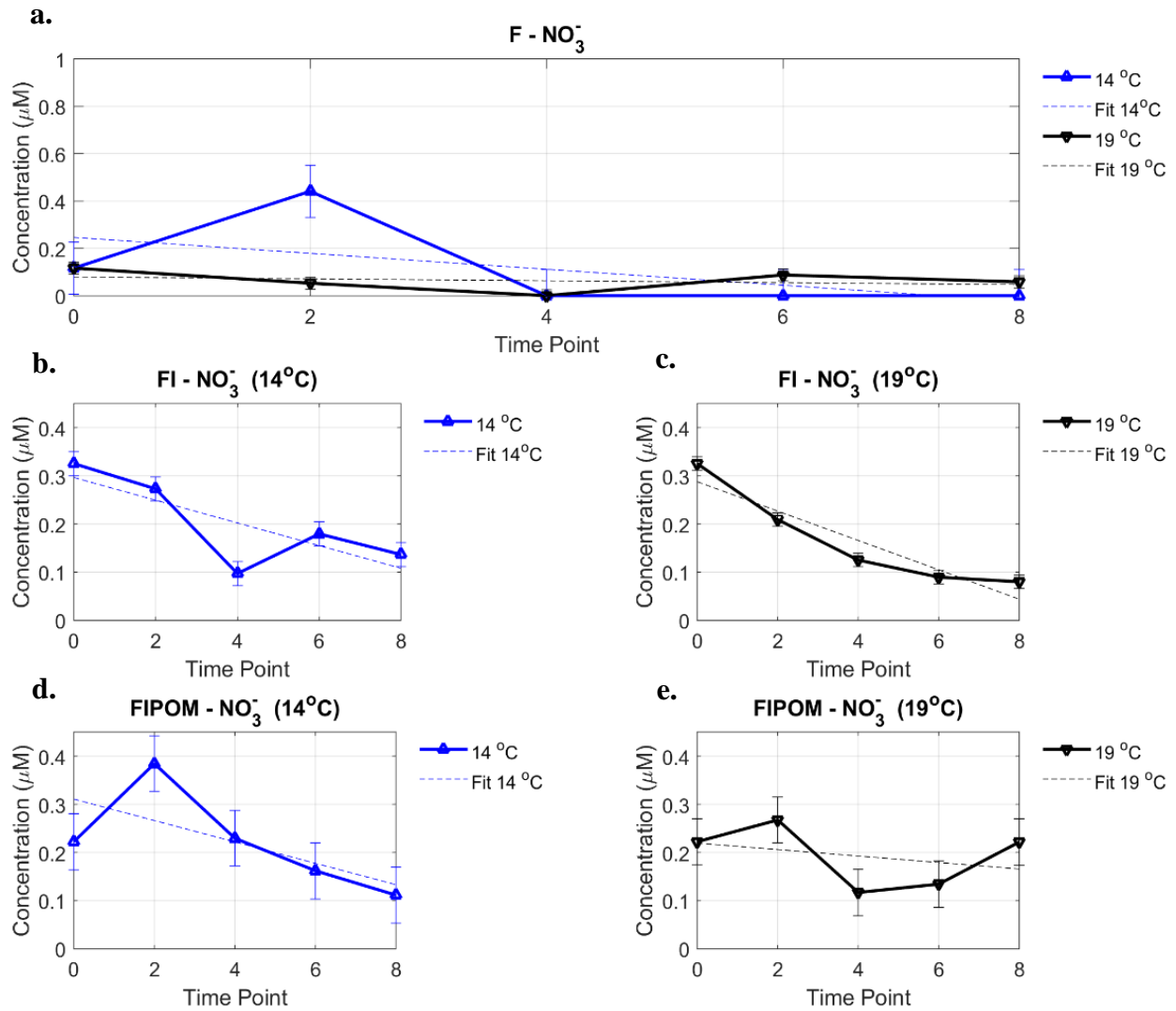


Figure 6: Nitrate concentrations for F, FI, and FIPOM. Error bars (a): ± 0.11 (14°) and ± 0.025 (19°), (b): ± 0.025 , (c): ± 0.014 , (d): ± 0.058 , and (e): ± 0.048 .

Phosphate

The F treatment in the cooler temperature incubation had remained relatively flat (no change) over the duration of the experiment and the warmer temperature incubation had an overall net production ($0.009 \pm 0 \mu\text{M}/\text{day}$, $\Delta = 0.0396 \mu\text{M}$; Figure 7). Both temperature incubations in FI – PO_4^{3-} had an overall net consumption ($-0.003 \pm 0.002 \mu\text{M}/\text{day}$, $\Delta = -0.0176 \mu\text{M}$ (14°); and $-0.002 \pm 0.002 \mu\text{M}/\text{day}$, $\Delta = -0.0249 \mu\text{M}$ (19°)). FI – PO_4^{3-} 14 and FI – PO_4^{3-} 19 concentrations over the duration of the experiment were significantly different from one another ($p = 0.042$). For both temperature incubations in FIPOM – PO_4^{3-} , there was an overall net production of phosphate

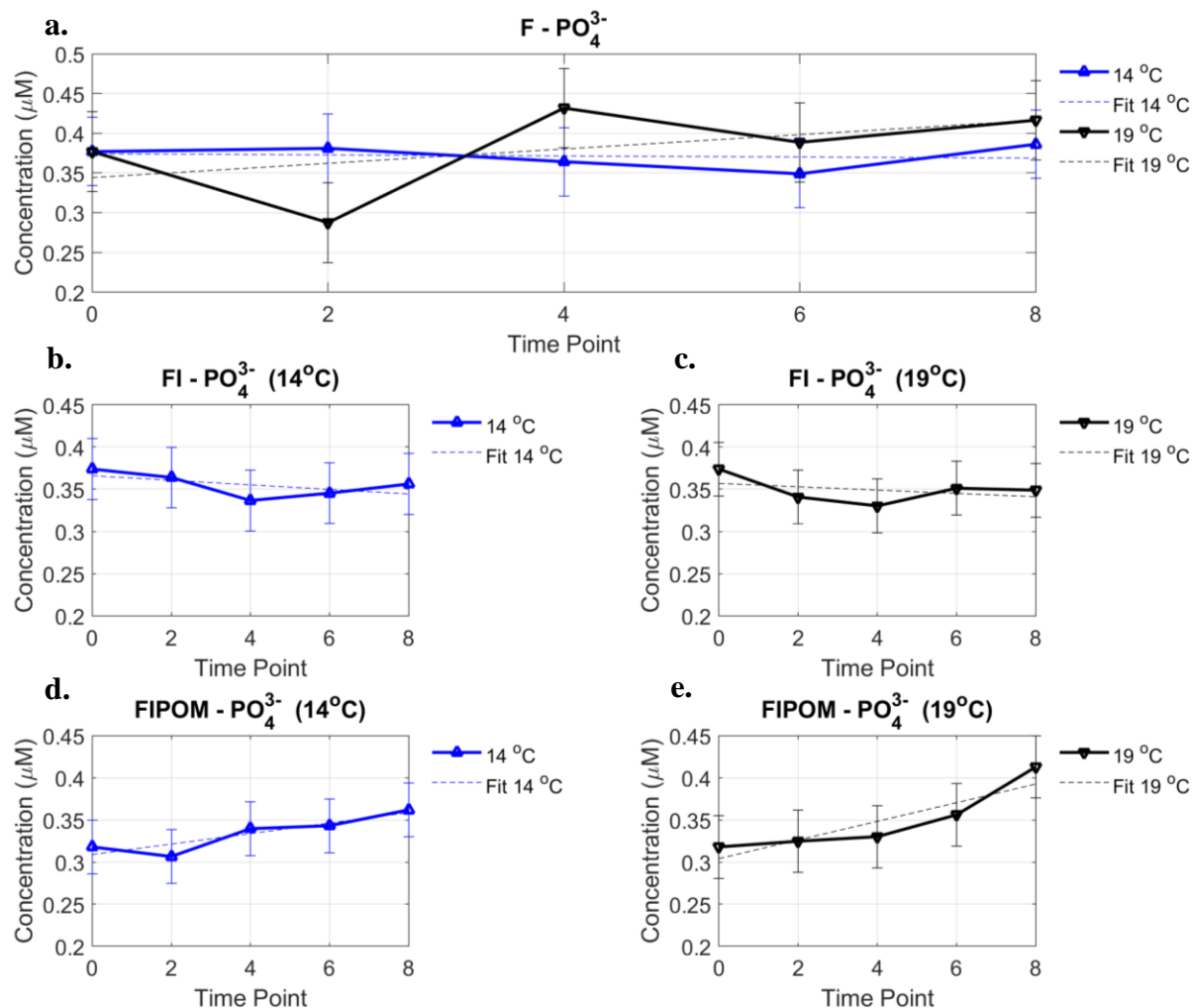


Figure 7: Phosphate concentrations for F, FI, and FIPOM. Error bars (a): ± 0.043 (14°) and ± 0.05 (19°), (b): ± 0.036 , (c): ± 0.032 , (d): ± 0.032 , and (e): ± 0.037 .

($0.006 \pm 0.001 \mu\text{M}/\text{day}$, $\Delta = 0.044 \mu\text{M}$ (14°); and $0.011 \pm 0.003 \mu\text{M}/\text{day}$, $\Delta = 0.095 \mu\text{M}$ (19°)), with the warmer temperature incubation having a faster production rate and larger delta. FIPOM – PO_4^{3-} 14 and FIPOM – PO_4^{3-} 19 concentrations over the duration of the experiment were significantly different from one another ($p = 0.049$).

Ratios

Figure 8 illustrates the stoichiometry of the expected ratio of OM from the Redfield ratio (6.6 C: 1 N and 16 N: 1 P), the initial time point (T_0), the delta of the OM consumed for both incubation temperatures, and the final time point (T_8) for both incubation temperatures. C:N ratios

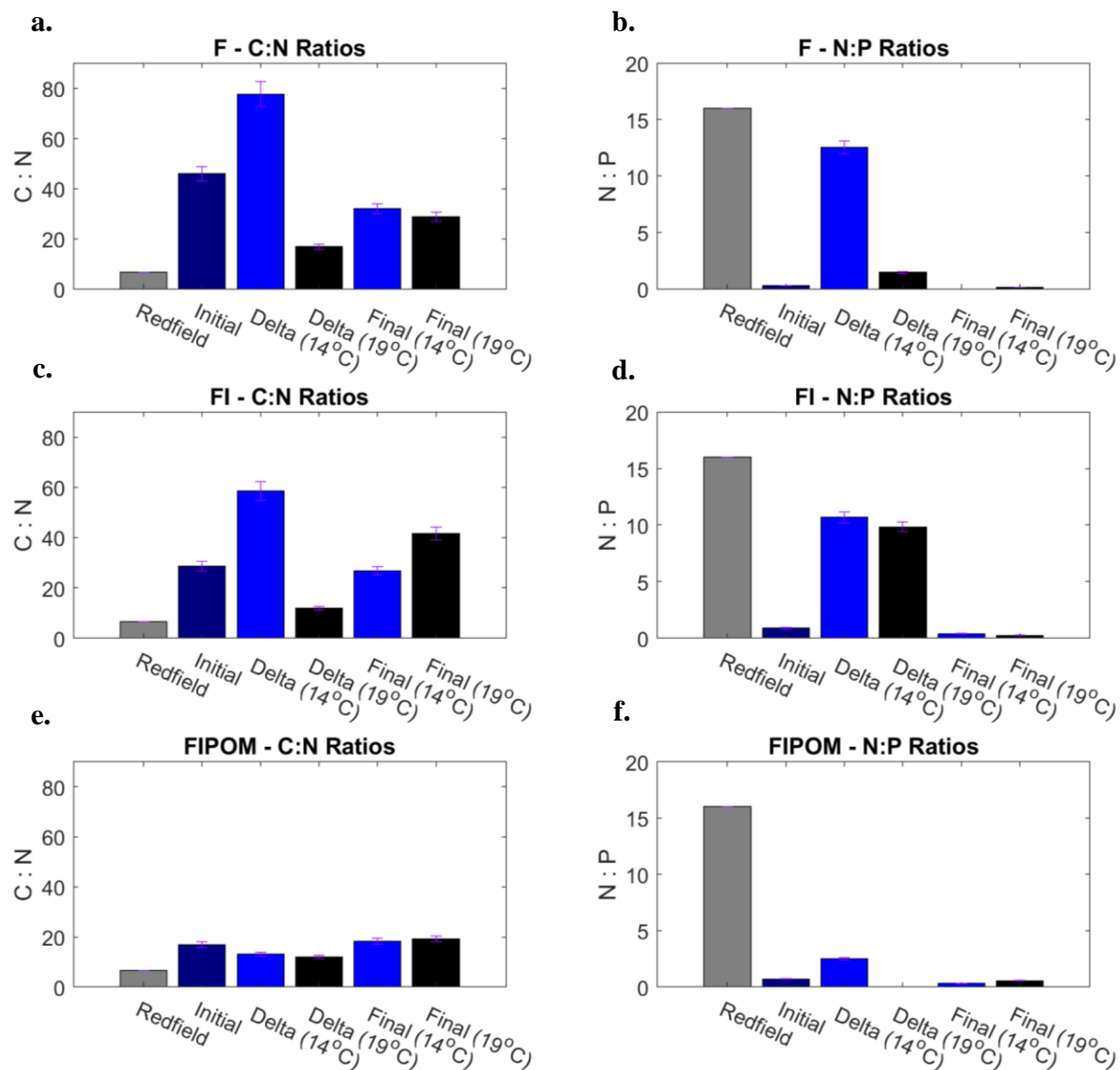


Figure 8: C:N ratios determined from POC and PON pool. N:P ratios determined from dissolved nitrate and phosphate pools. Error bars for (a): $\pm 6.4\%$, (b): $\pm 4.4\%$, (c): $\pm 6.4\%$ (d): $\pm 4.4\%$, (e): $\pm 6.4\%$, and (f): $\pm 4.4\%$.

were calculated based on the POC and PON pools and the N:P ratios were calculated from the dissolved inorganic NO_3^- and PO_4^{3-} pools. For the F treatments, the initial OM had a stoichiometric ratio of 45.8 C: 1 N and 0.31 N: 1 P. In the cooler temperature incubation, the delta stoichiometry the warmer temperature incubation, the delta stoichiometry was 16.8 C: 1 N and 1.47 N: 1 P, with the final ratio of 28.7 C: 1 N and 0.14 N: 1 P. The FI treatments initial OM ratio was 28.65 C: 1 N and 0.87 N: 1 P. In the cooler temperature incubation, the delta stoichiometry was 58.67 C: 1 N

and 10.68 N: 1 P, with the final ratio of 26.75 C: 1 N and 0.38 N: 1 P. The warmer temperature incubation had a delta stoichiometric ratio of 11.92 C: 1 N and 9.84 N: 1 P, with a final ratio of 41.62 C: 1 N and 0.23 N: 1 P. The FIPOM treatments had an initial OM ratio of 16.88 C: 1 N and was 77.69 C: 1 N and 12.54 N: 1 P, with the final ratio of 31.95 C: 1 N and 0 N: 1 P. Whereas in 0.70 N: 1 P. The cooler temperature incubation had a delta ratio of 13.11 C: 1 N and 2.52 N: 1 P, with a final ratio of 18.19 C: 1 N and 0.3 N: 1 P. In the warmer temperature incubation, the delta had a stoichiometry of 11.95 C: 1 N and 0.006 N: 1 P, with a final ratio of 19.16 C: 1 N and 0.53 N: 1 P.

2020 Experiment

Particles

Figure 9 illustrates the particles concentrations (particles per mL) for the F and FIPOM

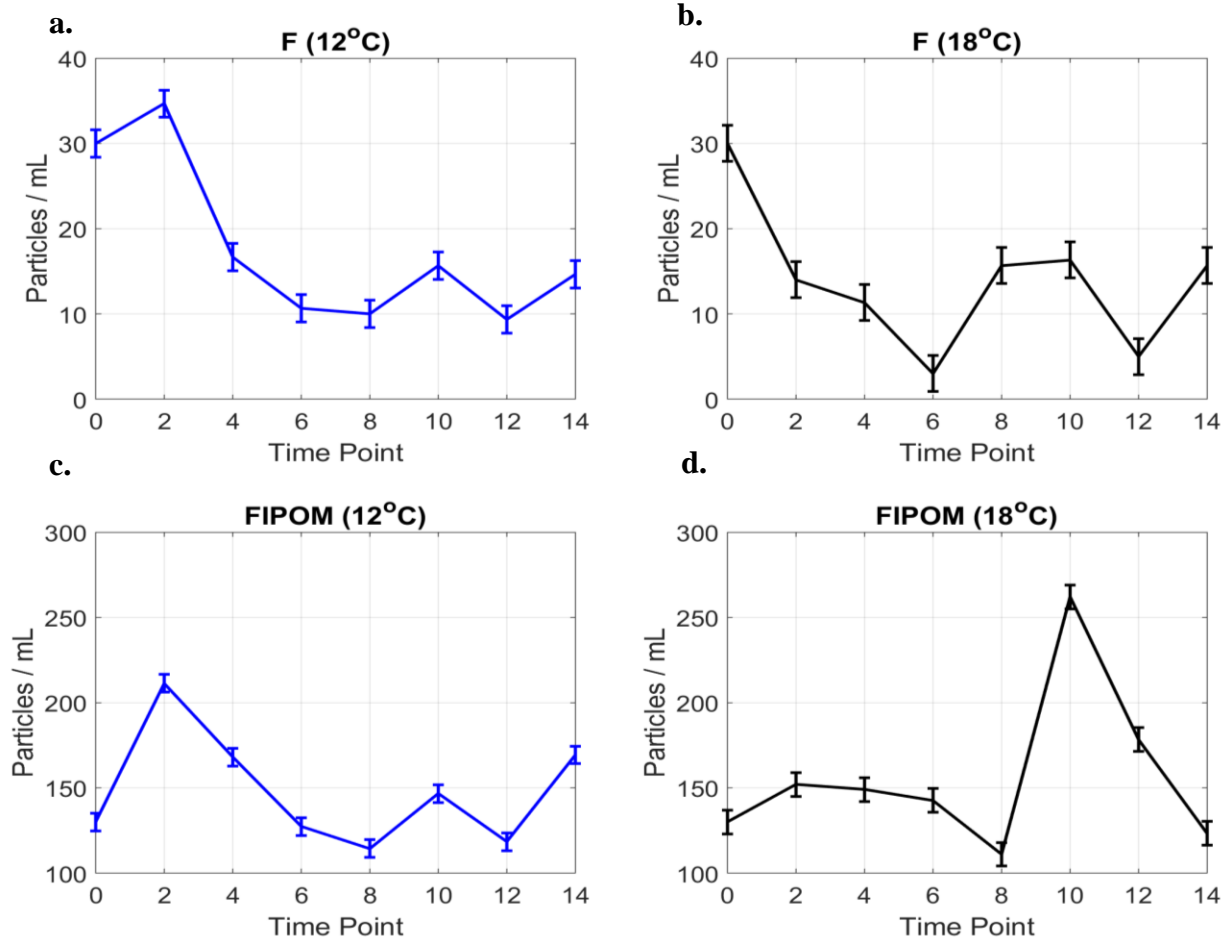


Figure 9: Particles/mL for F and FIPOM in each incubation. Error bars (a): ± 1.6 , (b): ± 2.11 , (c): ± 5.16 , and (d): ± 6.94 .

treatments. Initial conditions for the F treatment had 30 particles/mL, whereas the FIPOM had 130 particles/mL. Over the course of the experiment, the number of particles in both F temperature incubation treatments decreased (14.6 particles/mL and 15.6 particles/mL for in situ and experimental, respectively). FIPOM exhibited fluctuations in the number of particles/mL, with the final particles being 169.3 particles/mL for the cooler temperature incubation and 123.3 particles/mL for the warmer temperature incubation. Over the course of the experiment, the average area of particles increased (Figure 10). Particles in the F treatment were almost two times the size as the particles in the FIPOM treatment. Pictures from the FlowCAM of particles from T₂ and T₁₄ displayed in Table 3.

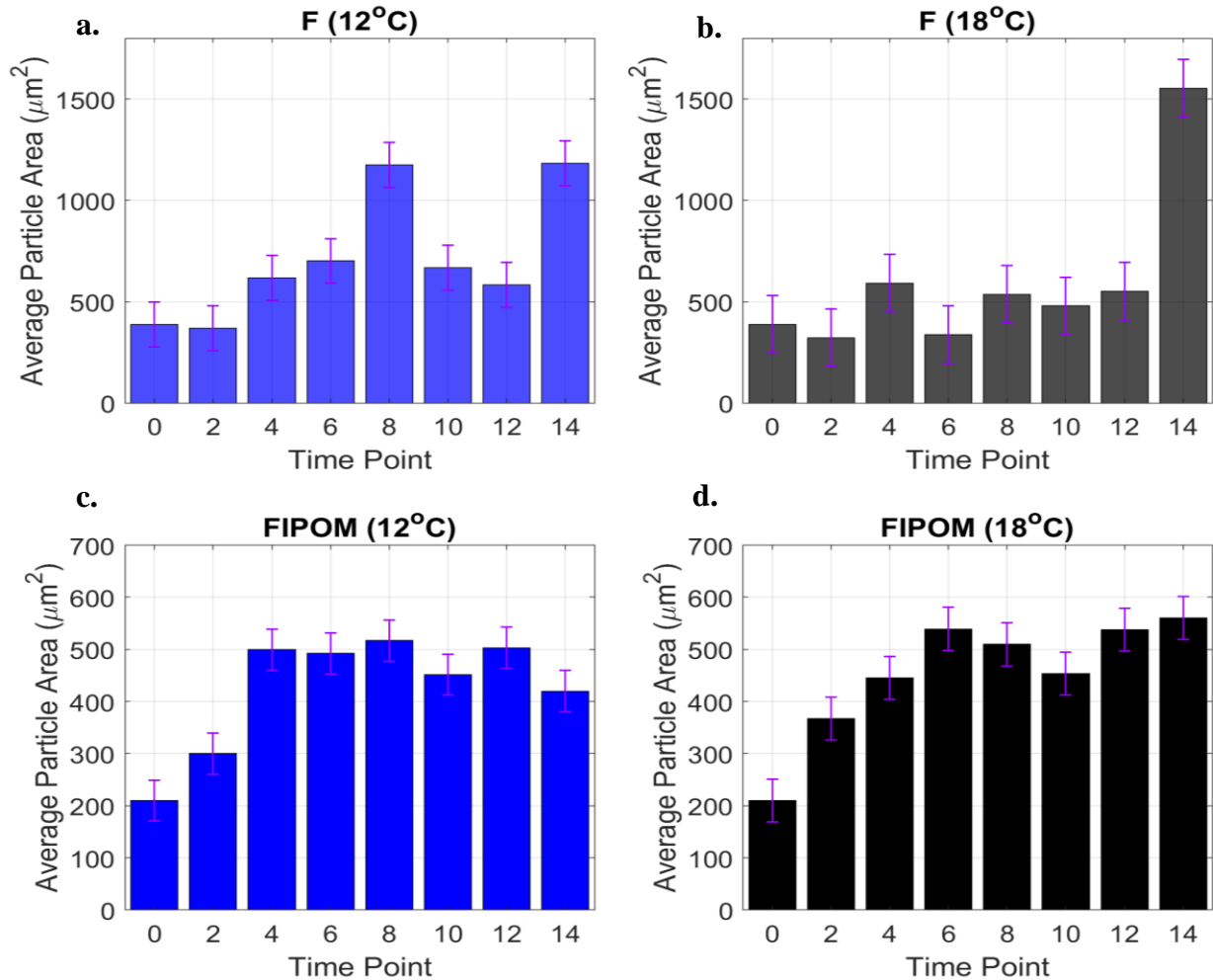

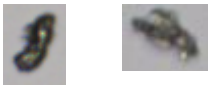




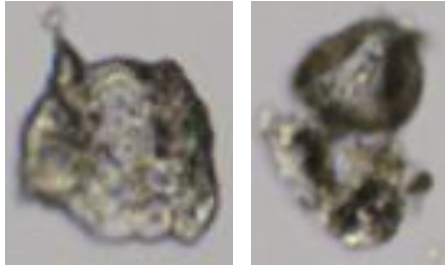



Figure 10: Average particle area (μm^2) for F and FIPOM incubations. Note F axes are not the same as the FIPOM axes. Error bars (a): ± 110.74 , (b): ± 141.41 , (c): ± 39.45 , and (d): ± 41.35 .

Table 3: FlowCAM pictures of particles from T₂ and T₁₄ for F and FIPOM treatments at both incubation temperatures.

Time Point	Treatment	
T ₂	F – 12°C 	FIPOM – 12°C 
	F – 18°C 	FIPOM – 18°C 
T ₁₄	F – 12°C 	FIPOM – 12°C 
	F – 18°C 	FIPOM – 18°C 

Cell counts

Although the F treatment was filtered through a 0.2-µm capsule filter and the average bacterial cell is 2 – 3 µm, the initial cell counts were 7.88×10^5 per mL and the FIPOM treatment initially had 7.08×10^5 per mL (Figure 11). As seen in both treatments and temperature incubations, there was a large and rapid population decrease (crash) of 33 - 51% that occurred prior to incubation termination at 14 days. Timing of the population crashes in the experimental temperature incubation treatments occurred before the in situ temperature incubation treatments. Population regrowth was observed after the crash and was faster in FIPOM – 18 compared to FIPOM – 12. The cell count trends are temporally related to the trends seen in the subsequent elemental pools (see below).

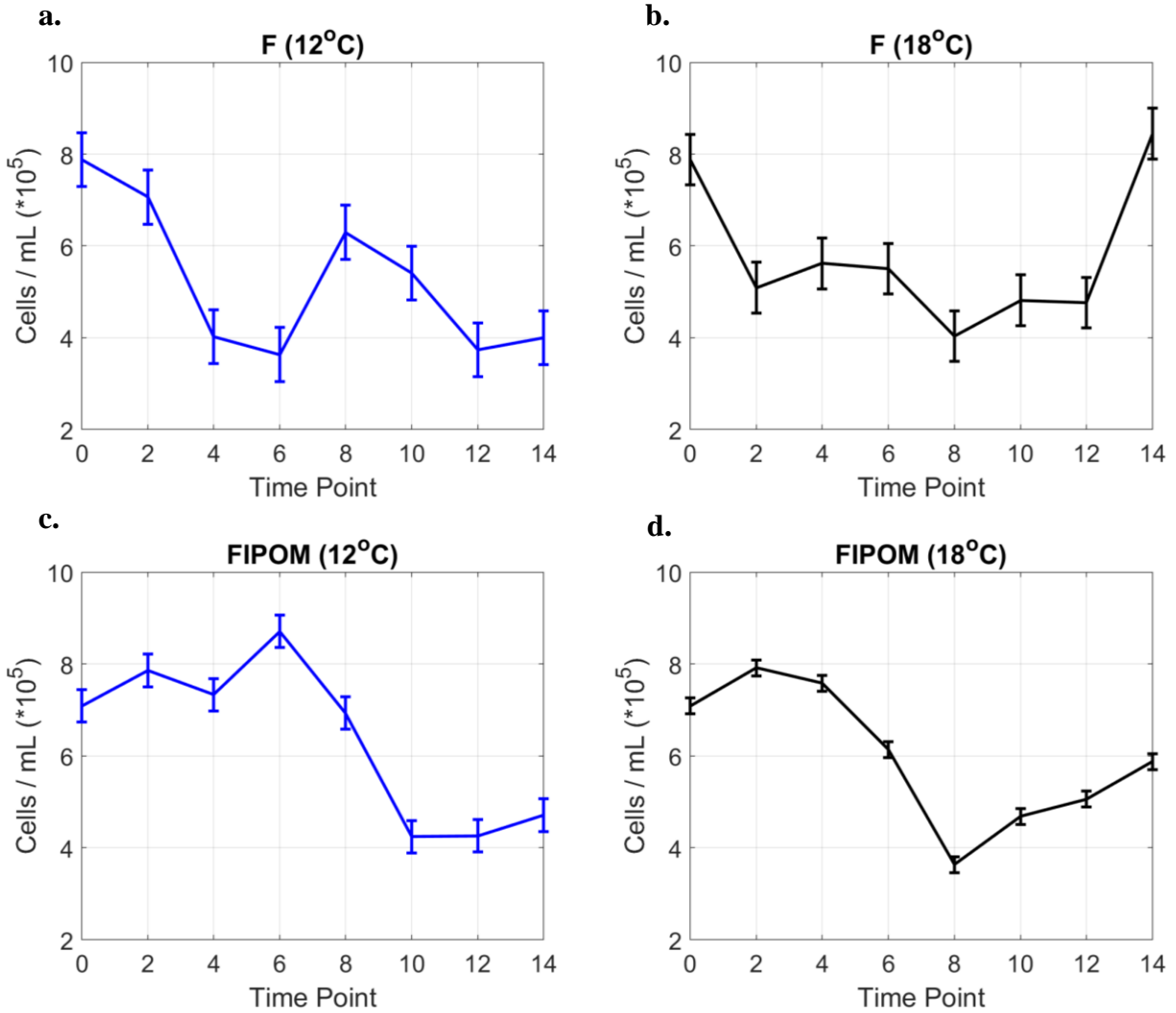


Figure 11: Cell counts/mL (*10⁵) for F and FIPOM in each incubation. Error bars (a): ± 0.587 , (b): ± 0.553 , (c): ± 0.353 , and (d): ± 0.173 .

Table 4 summarizes results from the 2020 experiment, presenting for T₀ – T₁₄: rates and uncertainty ($\mu\text{M}/\text{day}$), overall difference from T₁₄ to T₀ in concentration to determine net consumption or production (Δ ; μM), t – test calculated from the slope of the linear regression and uncertainty to determine if the rate was significantly different than 0 ($p < 0.05$), and the statistical significance from ANOVA Two – Factor without Replication if the measured concentrations of an elemental pool for each treatment was significantly different from one another ($p < 0.05$).

Table 4: Rate and uncertainty ($\mu\text{M}/\text{day}$), delta (Δ ; μM), t – test to determine if rate is significantly different than 0 with a 95% confidence level ($p < 0.05$), and ANOVA p – value for the 2020 experiment concentrations from $T_0 - T_{14}$ with a 95% confidence level ($p < 0.05$). Bolded p – values are significantly different.

Sample ID	Rate ($\mu\text{M}/\text{day}$) \pm Uncertainty in Rate ($\mu\text{M}/\text{day}$)	Delta (Δ ; μM)	t – test p – value of rate	ANOVA [In situ] vs [Experimental] p - value
F – C 12	-0.282 ± 0.476	-7.86	0.30	0.193
F – C 18	0.319 ± 0.476	11.30	0.31	
FIPOM – C 12	-0.652 ± 0.273	-12.36	0.07	0.028
FIPOM – C 18	-0.628 ± 0.322	-14.84	0.09	
F – N 12	-0.004 ± 0.010	-0.143	0.37	0.287
F – N 18	0.001 ± 0.006	-0.035	0.29	
FIPOM – N 12	-0.031 ± 0.008	-0.329	0.03	0.009
FIPOM – N 18	-0.034 ± 0.008	-0.299	0.03	
F – P 12	0.001 ± 0.000	0.006	0.14	0.467
F – P 18	0.000 ± 0.000	0.013	0.14	
FIPOM – P 12	-0.002 ± 0.001	-0.026	0.03	0.001
FIPOM – P 18	-0.002 ± 0.001	-0.022	0.04	
F – NO_3^- 12	-0.010 ± 0.004	-0.139	0.05	0.034
F – NO_3^- 18	-0.009 ± 0.004	-0.204	0.06	
FIPOM – NO_3^- 12	-0.001 ± 0.005	-0.126	0.41	0.011
FIPOM – NO_3^- 18	-0.004 ± 0.004	-0.151	0.19	
F – PO_4^{3-} 12	-0.001 ± 0.001	-0.015	0.37	0.925
F – PO_4^{3-} 18	-0.001 ± 0.002	-0.007	0.41	
FIPOM – PO_4^{3-} 12	0.004 ± 0.003	-0.021	0.13	0.854
FIPOM – PO_4^{3-} 18	0.002 ± 0.003	0.098	0.32	

Carbon

In the F treatment, the POC concentrations increased until time point 10, where both temperature incubations exhibited a rapid decrease to time point 12. The cooler temperature incubation saw POC decrease further to the final time point, resulting in an overall net consumption (-0.282 ± 0.476 ($\mu\text{M}/\text{day}$), $\Delta = -7.86$ μM ; Table 4, Figure 12). On the other hand, the warmer temperature incubation exhibited an increase in POC from T_{12} to the final time point (T_{14}), which resulted in an overall net production (0.319 ± 0.476 ($\mu\text{M}/\text{day}$), $\Delta = 11.30$ μM). Both FIPOM – C temperature incubations had an overall net consumption (-0.652 ± 0.273 ($\mu\text{M}/\text{day}$), $\Delta = -12.36$ μM (12°); -0.628 ± 0.322 ($\mu\text{M}/\text{day}$), $\Delta = -14.84$ μM (18°)). These trends are the same as the 2019

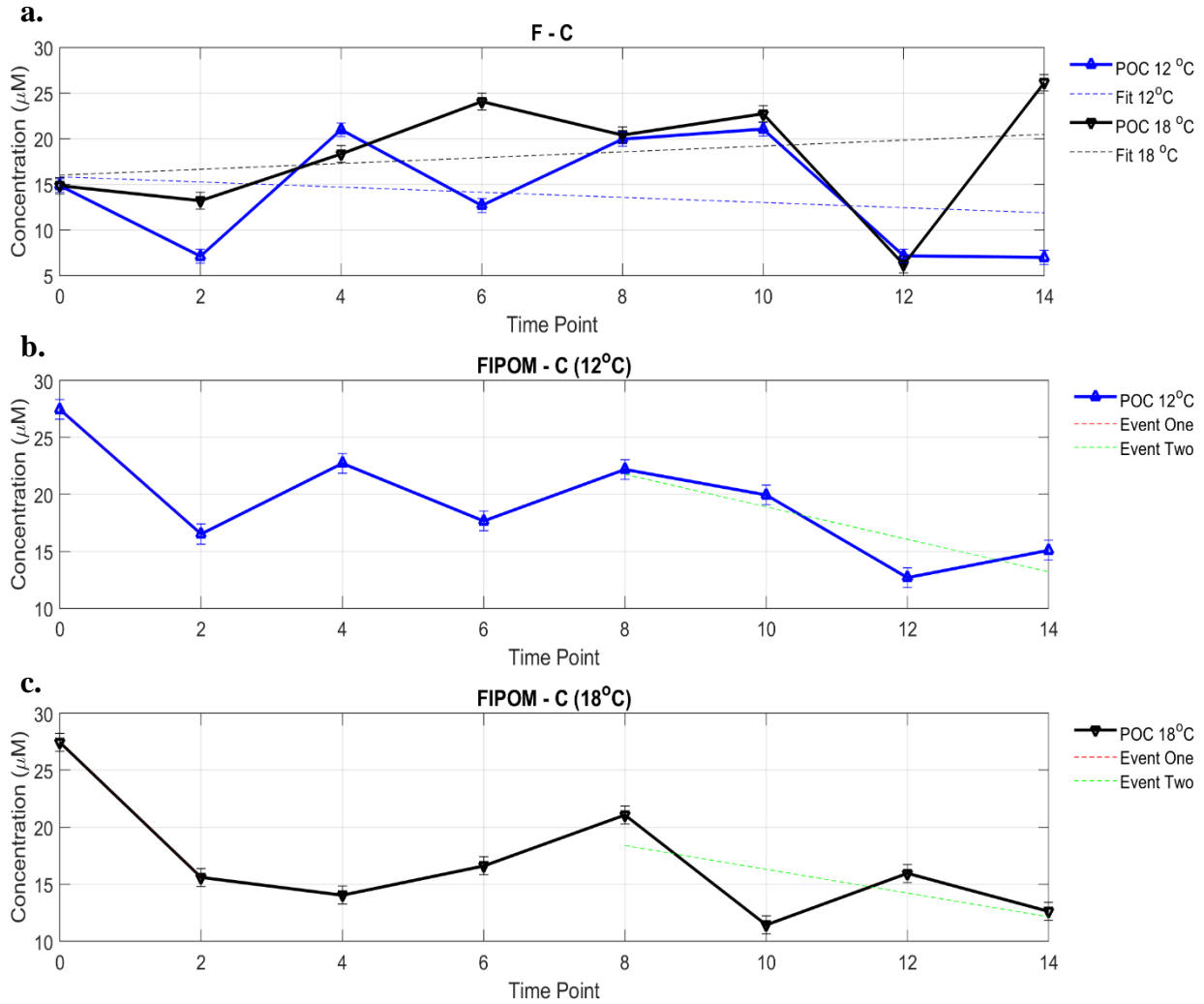


Figure 12: Carbon concentrations for F and FIPOM. Event One ($T_0 - T_2$) and Event Two ($T_8 - T_{14}$) illustrated in FIPOM. Error bars for (a) ± 0.75 (12°) and ± 0.91 for 18, (b): ± 0.87 , and (c): ± 0.79 .

experiment where the F treatment exhibited POC consumption at cooler temperatures and POC production at warmer temperatures, and FIPOM consumption for both temperature incubations. The trends in POC concentrations in FIPOM – C can be broken up into two events, as there were two consumption events ($T_0 - T_2$ and $T_8 - T_{14}$). The warmer temperature incubation had a faster consumption rate ($-5.93 \pm 0.00 \mu\text{M}/\text{day}$) in Event One and a larger consumption ($-11.85 \mu\text{M}$) than the cooler temperature incubation ($-5.47 \pm 0.00 \mu\text{M}/\text{day}$) and consumption ($-10.93 \mu\text{M}$). In Event Two, the cooler temperature incubation had a faster consumption rate ($-1.43 \pm 0.52 \mu\text{M}/\text{day}$) than the warmer temperature incubation ($-1.04 \pm 0.75 \mu\text{M}/\text{day}$) but had a larger consumption (-8.46

μM) than the cooler temperature incubation ($-7.09 \mu\text{M}$). FIPOM – C 12 and FIPOM – C 18 concentrations over the duration of the experiment were significantly different than one another ($p = 0.028$). POC consumption and production inversely correlated to cell counts ($R^2 = 1$). When the cells per mL increase, POC concentrations decrease; when the cells per mL decrease, POC concentrations increase, as illustrated from T_6 to T_8 in both temperature incubations.

Nitrogen

The only treatment that exhibited PON production was F – N 18 ($0.001 \pm 0.006 \mu\text{M/day}$), with the other three treatments exhibiting PON consumption (Table 4, Figure 13). All four treatments had an overall net consumption. FIPOM – N 12 ($-0.031 \pm 0.008 \mu\text{M/day}$, $\Delta = -0.329 \mu\text{M}$) and FIPOM – N 18 ($-0.034 \pm 0.008 \mu\text{M/day}$, $\Delta = -0.299 \mu\text{M}$) concentrations over the

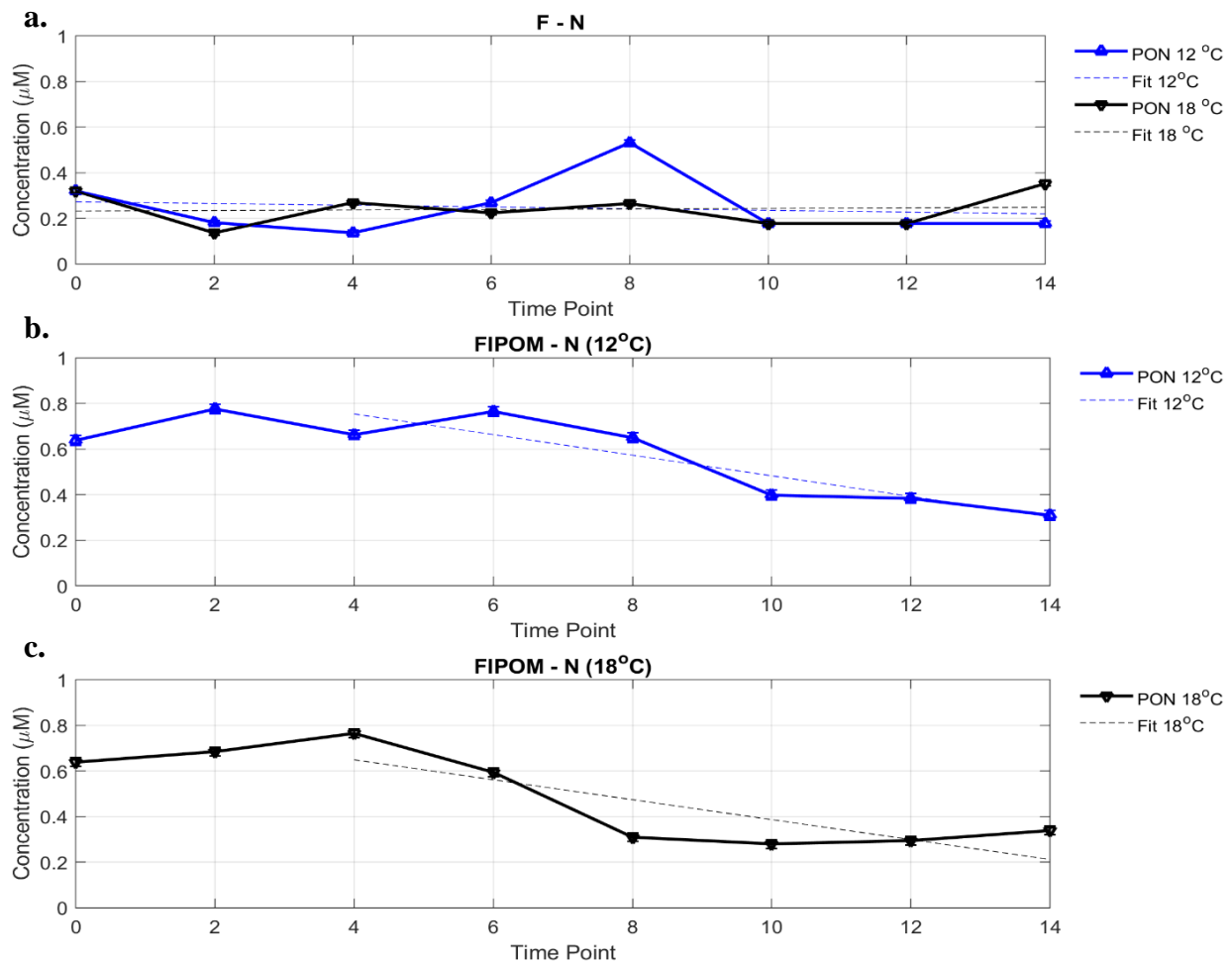


Figure 13: Nitrogen concentrations for F and FIPOM. Error bars for (a): ± 0.011 (12°) and ± 0.01 (18°), (b): ± 0.021 , and (c): ± 0.019 .

duration of the experiment were significantly different than one another ($p = 0.009$). FIPOM – N exhibited delayed PON consumption as compared to POC (Figure 12), starting at T_6 for the cooler temperature incubation and T_4 for the warmer temperature incubation. Linear regression analysis of the PON consumption rate was started at T_4 for both treatments to keep them comparable. After the initiation of PON consumption at T_4 , the cooler temperature incubation had a faster consumption rate ($-0.0452 \pm 0.01 \mu\text{M}/\text{day}$ versus $-0.0437 \pm 0.014 \mu\text{M}/\text{day}$), and the warmer temperature incubation had a larger net consumption ($\Delta = -0.426 \mu\text{M}$ versus $\Delta = -0.353 \mu\text{M}$).

Phosphorus

The POP concentration in the F – P treatment stayed relatively linear throughout the

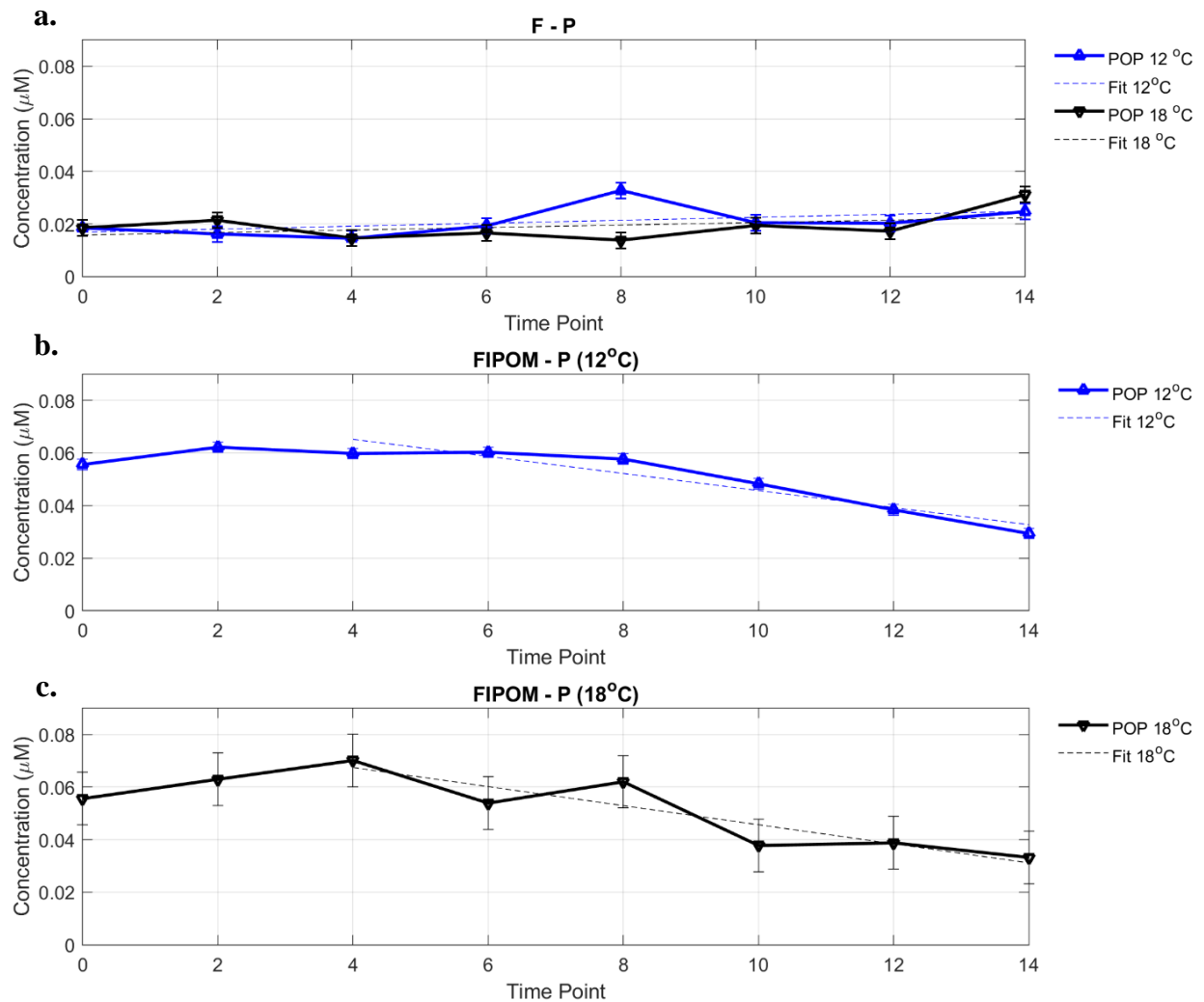


Figure 14: Phosphorus concentrations for F and FIPOM. Error bars for (a): ± 0.003 (12°) and ± 0.003 (18°), (b): ± 0.002 , and (c): ± 0.01 .

duration of the incubations with the warmer temperature having a slightly larger net production than the cooler temperature ($\Delta = 0.013$ (18°); $\Delta = 0.006$ (12°); Table 4, Figure 14). POP concentrations in the FIPOM – P treatments exhibited similar consumption trends for both temperature incubations with similar overall net consumption (-0.002 ± 0.001 ($\mu\text{M}/\text{day}$), $\Delta = -0.026$ μM (12°); -0.002 ± 0.001 ($\mu\text{M}/\text{day}$), $\Delta = -0.022$ μM (18°)). FIPOM – P 12 and FIPOM – P 18 concentrations over the duration of the experiment were significantly different than one another ($p = 0.001$). Similar to the FIPOM – N results, observed consumption was delayed relative to POC and/or PON, starting at T_8 for the cooler temperature incubation and T_4 for the warmer temperature incubation. Linear regression analysis of the POP consumption rate was started at T_4 to keep them comparable. After the initiation of POP consumption at T_4 , a faster consumption rate was observed at the warmer temperature (-0.0036 ± 0.001 $\mu\text{M}/\text{day}$) and larger net consumption (-0.037 μM) than the cooler temperature (-0.0032 ± 0.00 $\mu\text{M}/\text{day}$ and -0.030 μM , respectively).

Nitrate

All four treatments exhibited an overall net consumption of NO_3^- (Figure 15), similar to what was observed in the 2019 experiment NO_3^- pool and is the opposite of what was expected. The changes in the nitrate concentrations are inversely correlated ($R^2 = 1$) with the cell counts; when the cells per mL decrease, NO_3^- concentrations increase, as illustrated from T_8 to T_{10} in the cooler temperature incubation and T_6 to T_8 in the warmer temperature incubation. NO_3^- concentrations in the F – NO_3^- treatments exhibited similar consumption trends for both temperature incubations with the warmer temperature incubation exhibiting an overall net consumption (-0.010 ± 0.004 ($\mu\text{M}/\text{day}$), $\Delta = -0.1389$ μM (12°); -0.009 ± 0.004 ($\mu\text{M}/\text{day}$), $\Delta = -0.2039$ μM (18°); Table 4). In the warmer temperature FIPOM - NO_3^- incubation, there was a faster consumption rate and overall larger net consumption (-0.004 ± 0.004 ($\mu\text{M}/\text{day}$),

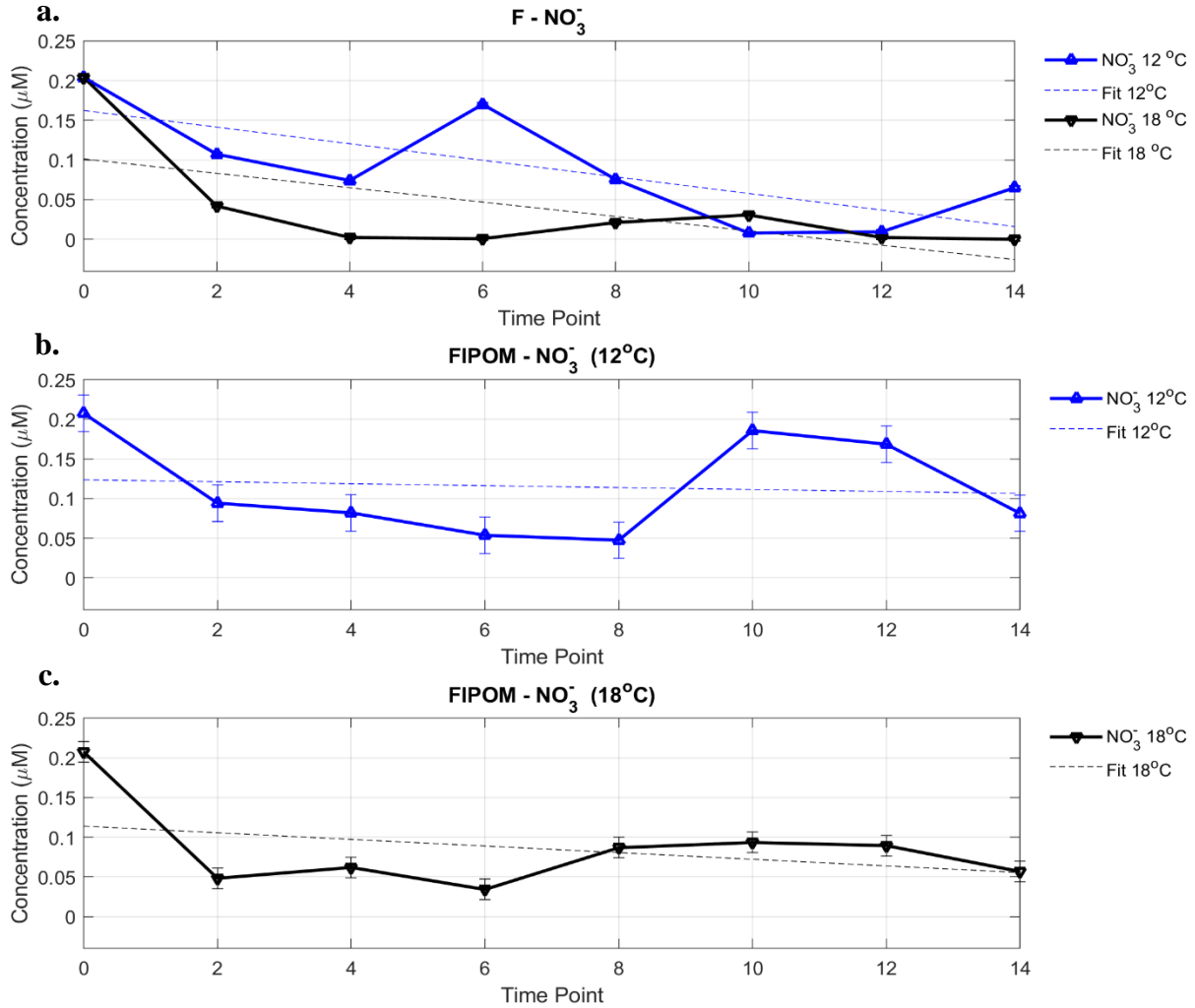


Figure 15: Nitrate concentrations for F and FIPOM. Error bars for (a): ± 0.002 (12°) and ± 0.002 (18°), (b): ± 0.021 , and (c): ± 0.013 .

$\Delta = -0.1507 \mu\text{M}$) than the cooler temperature incubation ($-0.001 \pm 0.005 (\mu\text{M}/\text{day})$, $\Delta = -0.1259 \mu\text{M}$). The F – NO₃⁻ 12 and F – NO₃⁻ 18 concentrations over the duration of the experiment were significantly different than one another ($p = 0.034$). Additionally, FIPOM – NO₃⁻ 12 and FIPOM – NO₃⁻ 18 concentrations over the duration of the experiment were significantly different than one another ($p = 0.011$)

Phosphate

Both F – PO₄³⁻ temperature treatments exhibited similar consumption trends and an overall net consumption of PO₄³⁻ ($-0.001 \pm 0.001 (\mu\text{M}/\text{day})$, $\Delta = -0.0152 \mu\text{M}$ (12°); -0.001 ± 0.002

($\mu\text{M}/\text{day}$), $\Delta = -0.0073 \mu\text{M}$ (18°); Table 4, Figure 16). As for the FIPOM - PO_4^{3-} treatments, both exhibited periods of PO_4^{3-} production and consumption. The cooler temperature incubation had an overall net consumption ($\Delta = -0.0207 \mu\text{M}$) whereas the warmer temperature incubation had an overall net production ($\Delta = 0.0978 \mu\text{M}$). Phosphate is also inversely correlated ($R^2 = 1$) to cell counts, similar to NO_3^- .

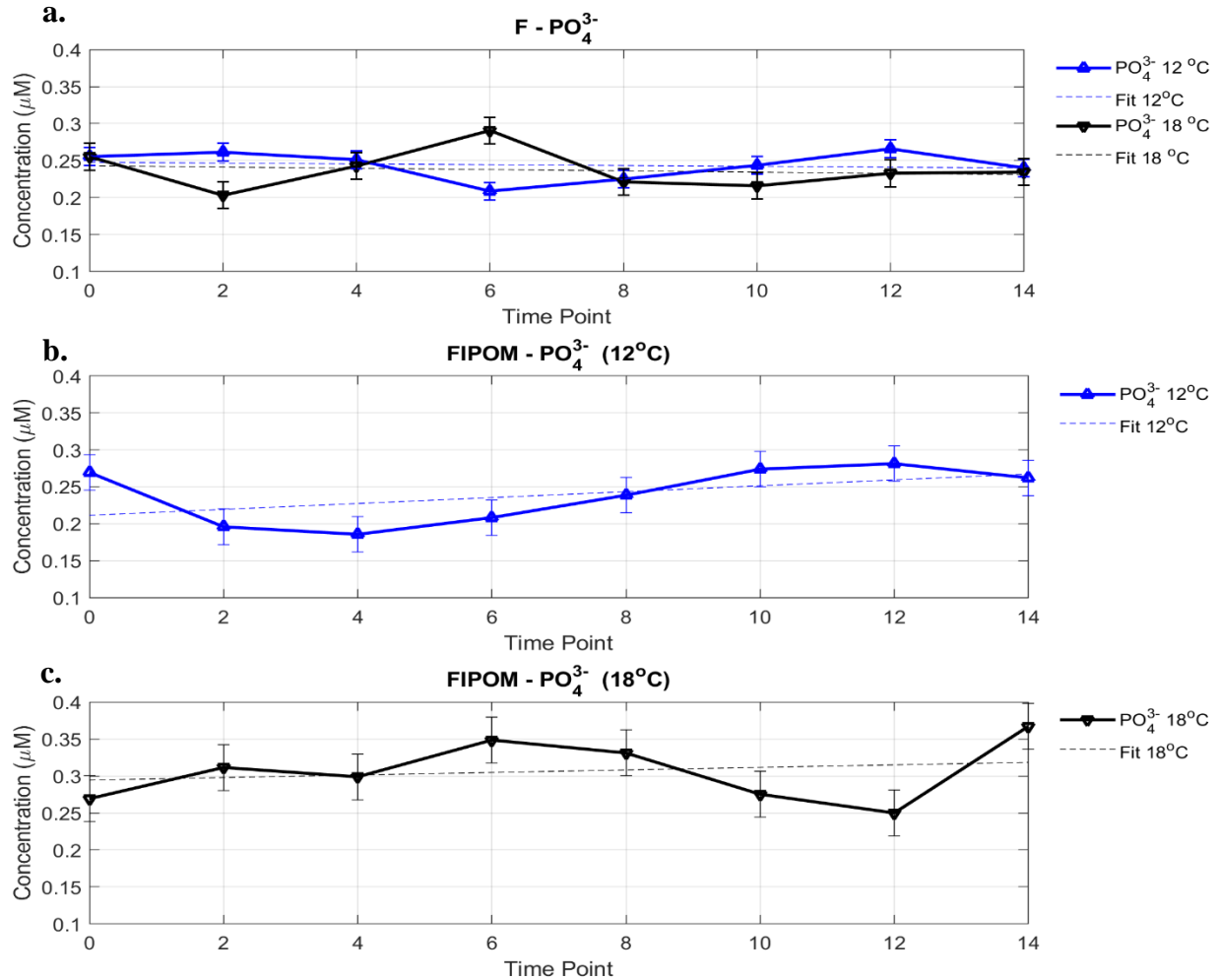


Figure 16: Phosphate concentrations for F and FIPOM. Error bars for (a): ± 0.012 (12°) and ± 0.016 (18°), (b): ± 0.024 , and (c): ± 0.031 .

Ratios

Figure 17 illustrates the stoichiometry of the expected ratio of OM from the Redfield ratio (6.6 C: 1 N, 16 N: 1 P, and 106 C: 1 P), the initial time point (T_0), the delta of the OM consumed for both incubation temperatures, and the final time point (T_8) for both incubation temperatures.

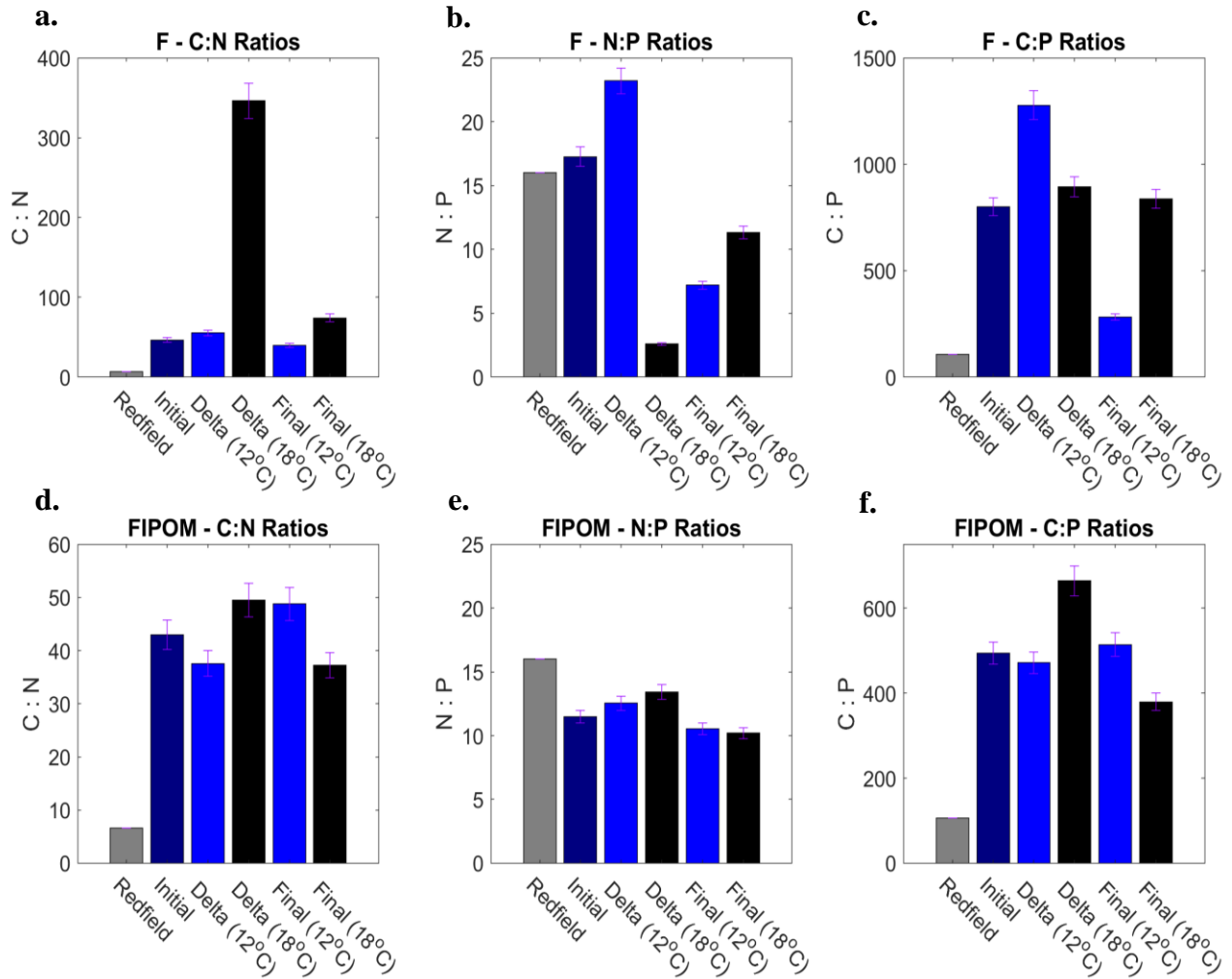


Figure 17: C:N:P ratios using POC, PON, and POP pools. Note the y-axis for F - C:N and F - C:P are not the same as FIPOM - C:N and FIPOM - C:P axes. Error bars for (a): $\pm 6.4\%$, (b): $\pm 4.4\%$, (c): $\pm 5.3\%$, (d): $\pm 6.4\%$, (e): $\pm 4.4\%$, and (f): $\pm 5.3\%$.

C:N:P ratios were calculated based on the POC, PON, and POP. For the F treatments, the initial OM had a stoichiometric ratio of 46.35 C: 1 N, 17.27 N: 1 P, and 800.56 C: 1 P. In the cooler temperature incubation, the delta stoichiometry was 55.07 C: 1 N, 23.21 N: 1 P, and 1278.11 C: 1 P, with the final ratio of 39.34 C: 1 N, 7.18 N: 1 P, and 282.68 C: 1 P. Whereas in the warmer temperature incubation, the delta stoichiometry was 346.38 C: 1 N, 2.58 N: 1 P, and 894.27 C: 1 P, with the final ratio of 74.1 C: 1 N, 11.31 N: 1 P, and 838.55 C: 1 P. The FIPOM treatments had an initial OM ratio of 43 C: 1 N, 11.48 N: 1 P, and 493.94 C: 1 P. The cooler temperature incubation had a delta ratio of 37.56 C: 1 N, 12.54 N: 1 P, and 471.2 C: 1 P, with the final ratio of 48.79 C: 1

N, 10.45 N: 1 P, and 514.28 C: 1 P. In the warmer temperature incubation, the delta had a stoichiometry of 49.49 C: 1 N, 13.41 N: 1 P, and 663.9 C: 1 P, with the final ratio of 37.26 C: 1 N, 10.18 N: 1 P, and 379.64 C: 1 P.

2019 to 2020 Experiment Comparison

Consumption or production rates for FIPOM of the respected elemental pool were compared for each experiment year to determine if the rate was statistically faster in the experimental temperature incubation than the in situ temperature incubation (Table 5). All rates used for comparison were from the full duration of the experiments, not the aforementioned events (POC) or delays (PON and POP) from 2020.

Table 5: Analysis of covariance determined if the rate of consumption/production in the experimental temperature incubation is significantly different than the rate of consumption/production in the in situ temperature incubation for the FIPOM elemental pools ($p < 0.05$).

Experiment Year	Comparisons	Elemental Pool	Covariance p - value
2019	Experimental (19°C) vs. In situ (14°C)	FIPOM – C	0.152
2019	Experimental (19°C) vs. In situ (14°C)	FIPOM – N	0.316
2019	Experimental (19°C) vs. In situ (14°C)	FIPOM – NO ₃ ⁻	0.429
2019	Experimental (19°C) vs. In situ (14°C)	FIPOM – PO ₄ ³⁻	0.165
2020	Experimental (18°C) vs. In situ (12°C)	FIPOM – C	0.955
2020	Experimental (18°C) vs. In situ (12°C)	FIPOM – N	0.795
2020	Experimental (18°C) vs. In situ (12°C)	FIPOM – P	1.000
2020	Experimental (18°C) vs. In situ (12°C)	FIPOM – NO ₃ ⁻	0.648
2020	Experimental (18°C) vs. In situ (12°C)	FIPOM – PO ₄ ³⁻	0.646

Carbon

The 2019 experiment exhibited both a faster consumption rate and larger delta concentration in the warmer temperature incubation than the cooler temperature incubation for POC (Figure 18). The rate of consumption in the warmer temperature incubation is not statistically different than the in situ temperature incubation, but there is an 84.4% of being different ($p = 0.156$, Table 5). The 2020 experiment saw similar rates of POC consumption but a larger delta concentration in the warmer temperature incubation. The rate of consumption between the in situ

and experimental temperature incubations are not statistically different from one another ($p = 0.955$, Table 5).

Nitrogen

The 2019 experiment exhibited a faster PON consumption and larger delta in the warmer temperature incubation than the cooler temperature incubation (Figure 19). However, rate of consumption in the warmer temperature incubation is not statistically different than the in situ temperature incubation ($p = 0.316$, Table 5). The 2020 experiment saw similar rates of PON consumption between the two incubation temperatures with a marginally larger delta in the cooler incubation. The rate of consumption between the in situ and experimental temperature incubations are not statistically different from one another ($p = 0.795$, Table 5).

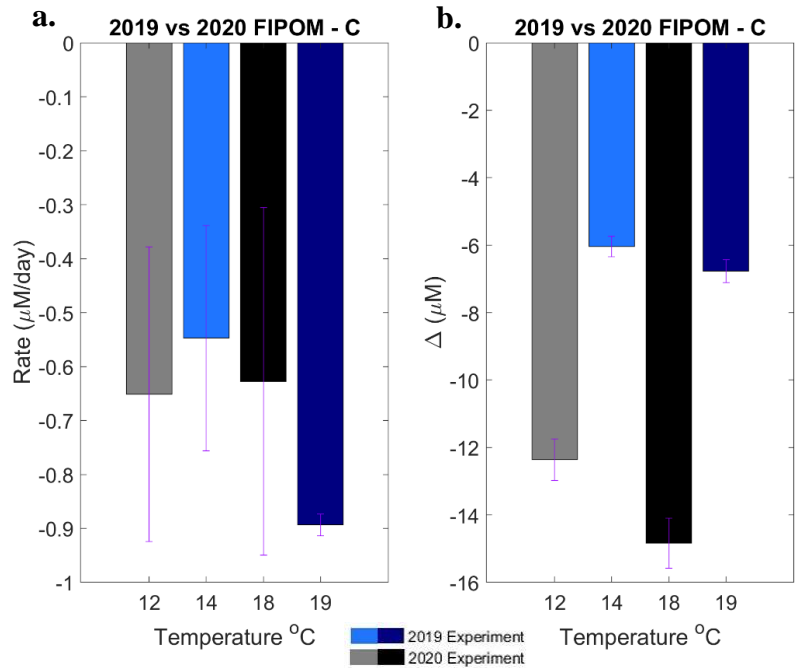


Figure 19: a. FIPOM - C 2019 rates versus 2020 rates. b. FIPOM - C 2019 deltas versus 2020 deltas. Error bars for (a) is the uncertainty in the fit: ± 0.273 (12°), ± 0.209 (14°), ± 0.322 (18°), and ± 0.02 (19°), and (b) is $\pm 5\%$ of the delta from analytical uncertainty.

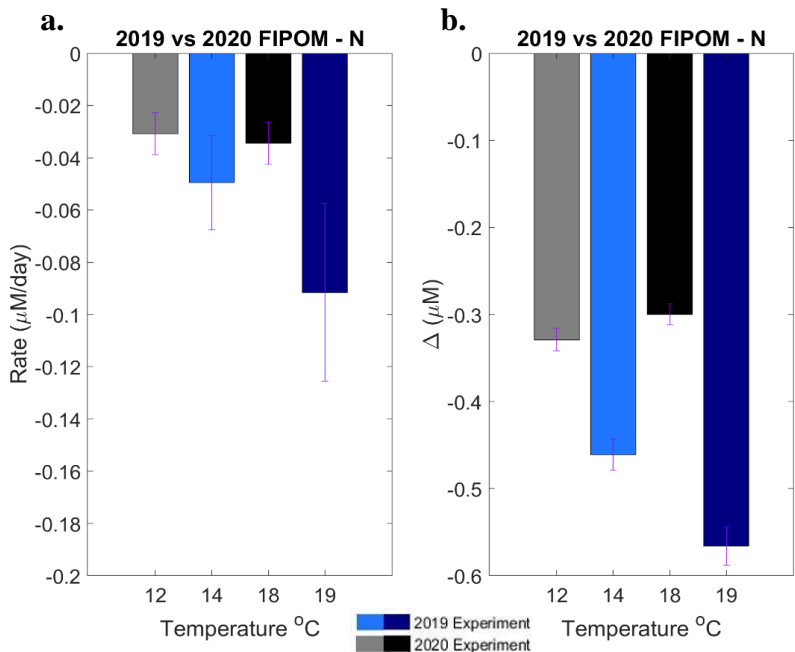


Figure 18: a. FIPOM - N 2019 rates versus 2020 rates. b. FIPOM - N 2019 deltas versus 2020 deltas. Error bars for (a) is the uncertainty in the fit: ± 0.008 (12°), ± 0.018 (14°), ± 0.008 (18°), and ± 0.034 (19°), and (b) is $\pm 4\%$ of the delta from analytical uncertainty.

Nitrate

The 2019 experiment exhibited a faster NO_3^- consumption rate and larger delta in the cooler temperature incubation than the warmer temperature incubation (Figure 20), with the rates of consumption not being statistically different ($p = 0.429$,

Table 5). Conversely, the 2020 experiment exhibited a faster NO_3^- consumption rate and

larger delta in the warmer incubation. Again, the rate of consumption was not statistically different ($p = 0.648$, Table 5).

Phosphate

The 2019 exhibited a faster PO_4^{3-} production rate and larger delta in the cooler temperature incubation than the warmer temperature incubation

(Figure 21). The rate of consumption in the warmer temperature incubation is not statistically

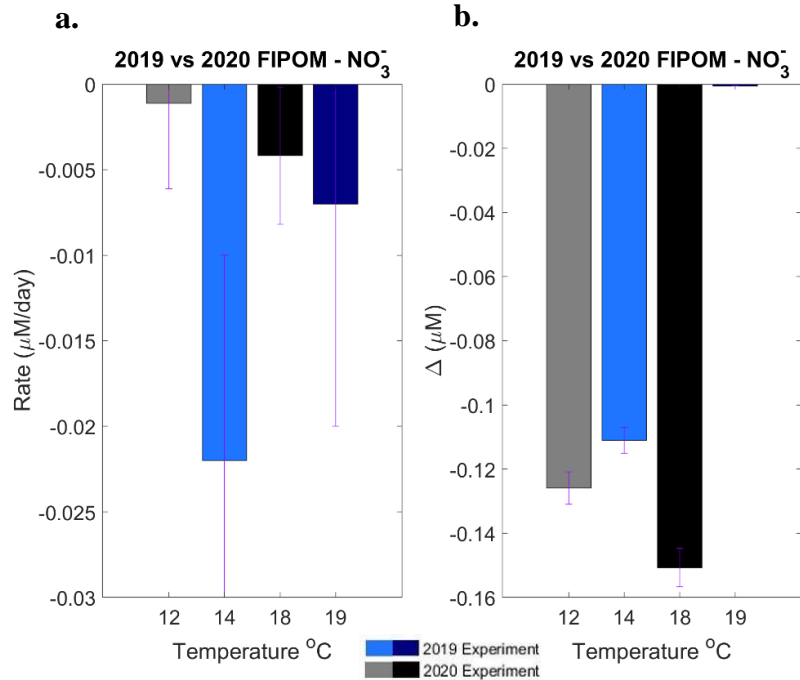


Figure 20: a. FIPOM - NO_3^- 2019 rates versus 2020 rates. b. FIPOM - NO_3^- 2019 deltas versus 2020 deltas. Error bars for (a) is the uncertainty in the fit: ± 0.005 (12°), ± 0.012 (14°), ± 0.004 (18°), and ± 0.013 (19°), and (b) is $\pm 4\%$ of the delta from analytical uncertainty.

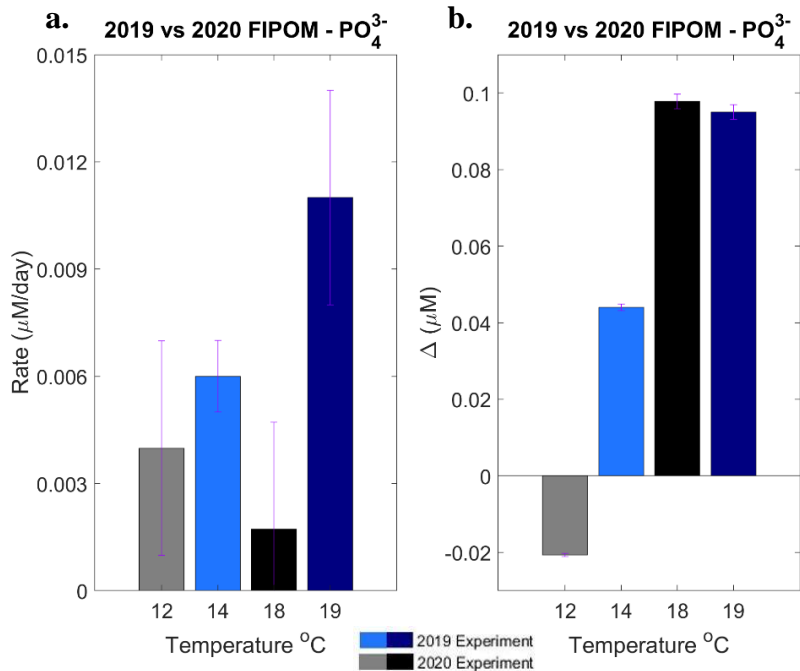


Figure 10: a. FIPOM - PO_4^{3-} 2019 rates versus 2020 rates. b. FIPOM - PO_4^{3-} 2019 deltas versus 2020 deltas. Error bars for (a) is the uncertainty in the fit: ± 0.012 (12°), ± 0.001 (14°), ± 0.013 (18°), and ± 0.003 (19°), and (b) is $\pm 2\%$ of the delta from analytical uncertainty.

different than the in situ temperature incubation, but there is an 83.5% of being different ($p = 0.165$, Table 5). The 2020 experiment exhibited a faster PO_4^{3-} production rate in the cooler temperature incubation but a larger delta in the warmer temperature incubation. The rates are not statistically different than one another ($p = 0.646$, Table 5).

Q₁₀

Estimates of the temperature coefficient (Q₁₀) computed using Eq. 3 for each elemental OM pool are presented in Table 6. During the 2019 experiment, the estimated Q₁₀ was greater than 2.0 for both carbon and nitrogen, yielding values of 2.66 ± 2.12 for POC and 3.42 ± 0.05 for PON. Whereas the 2020 experiment for each elemental pool overall and events/delays had a Q₁₀ value less than 2.0, yielding values of $\sim 0.6 - 1.1$ for POC, $\sim 0.7 - 1.2$ for PON, and $\sim 1.1 - 1.2$ for POP.

Table 6: Q₁₀ calculations for the FIPOM elemental pool for 2019 and 2020, with 2020 events (POC) and delays (PON and POP).

Year	FIPOM – Elemental Pool	Q ₁₀
2019	Carbon	2.66 ± 2.12
2019	Nitrogen	3.42 ± 0.05
2020	Carbon	0.94 ± 0.17
	Event One	1.14 ± 0.00
	Event Two	0.59 ± 0.36
2020	Nitrogen	1.21 ± 0.06
	Delay	0.70 ± 0.16
2020	Phosphorus	1.13 ± 0.07
	Delay	1.20 ± 0.39

DISCUSSION

Overall, we found strong support for our hypotheses that in warmer temperatures there were faster rates of consumption and an overall larger amount of OM consumed than in the cooler temperatures for POC, PON, and POP, largely confirming the predictions from the metabolic theory of ecology (Brown et al., 2004) and those specific to marine plankton (Lopez – Urrutia et al., 2006; Regaudie-de-Gioux and Duarte, 2012). Consumption in the FIPOM carbon elemental pool was observed immediately following incubation initiation, presumably due to an efficient

BGE and allocating organic carbon to building biomass before and after the population crash. The consumption in the nitrogen pool was delayed by one to two time points after carbon (2 – 4 days), and consumption in the phosphorus pool was further delayed one to two time points after nitrogen (2 – 4 days), with the cooler temperature experiencing the longer delay than the warmer temperature.

Within the warmer F – C treatments, there was an increase of carbon throughout the duration of the experiment, presumably due to the production of transparent exopolymer particles (TEP). TEP are sticky gel like particles, primarily composed of exo-polysaccharides generated by phytoplankton and bacteria that abiotically assemble in seawater, which are varying in size and provide surface area for the colonization of bacterial communities (Passow, 2002). Due to the stickiness of TEP, particles increase in size with time as other aggregates bind to it. This was seen in Figure 9a and 9b with the increasing area of particles for the 2020 warmer F – C treatment and visually in Table 3 from the FlowCAM images. TEP in the Gulf of Maine needs further investigation as it can be a large contributor to the marine carbon cycle (Passow, 2002). In the F treatments for C, N, and P, there was only one filter per time point, possibly creating bias at time points. There were also samples in PON that were close and below the level of detection limit, adding bias.

It is expected that the stoichiometric ratio for C:N, N:P, and C:P of the delta concentrations, which quantify the stoichiometry of the organic matter consumed over the course of the incubation, would be less than the ratio of the initial water conditions for both incubation temperatures, as marine heterotrophs are believed to preferentially consume nutrient rich organic matter (Schneider et al., 2003). The resulting stoichiometry of the OM left behind at the end of the incubations would thus be greater than both the initial and delta stoichiometry following mass

balance. If the delta stoichiometry is less than the initial ratio, then the element in the numerator of the ratio was preferentially left behind and the element in the denominator was preferentially consumed, and vice versa.

In 2019, the F and FI treatments for the cooler temperature C:N ratio, the delta stoichiometry exhibited a greater ratio than both the initial and the final ratio indicating carbon-rich material was preferentially consumed leaving nitrogen-rich OM behind (Figure 8). The warmer temperature incubation for the F, FI, and FIPOM treatments has a delta C:N ratio less than both the initial and the final ratio indicating nitrogen-rich OM was preferentially consumed leaving behind carbon-rich OM. In the cooler temperature F treatment and the warmer temperature FI and FIPOM treatments, the delta N:P ratio is less than both the initial and the final ratio indicating phosphate-rich OM was preferentially consumed leaving behind nitrate-rich OM. In the cooler temperature FI and FIPOM treatments and warmer temperature F treatment, the delta N:P ratio is greater than both the initial and the final ratio, indicating nitrate-rich OM was preferentially consumed leaving behind phosphate-rich OM. Overall, the initial C:N and N:P ratios were elevated compared to the expected Redfield ratio, indicating carbon-rich nitrogen-poor OM at in situ conditions.

For the 2020 experiment, in the F in situ treatment and the FIPOM experimental treatment, the C:N, N:P, and C:P stoichiometry of the delta concentrations exhibited a larger ratio than both the initial and the final ratio indicating carbon-rich OM was preferentially consumed leaving behind nitrogen-rich OM (Figure 17a, 17d), nitrogen-rich OM was preferentially consumed leaving behind phosphorus-rich OM (Figure 17b, 17e), and carbon-rich OM was preferentially consumed leaving behind phosphorus-rich OM (Figure 17c, 17f). The FIPOM in situ treatment had a delta C:N (Figure 17d) and C:P (Figure 17f) ratio less than the initial ratio indicating

nitrogen-rich OM and phosphorus-rich OM were preferentially consumed, leaving behind carbon-rich OM, respectively, and had a delta N:P (Figure 17e) ratio greater than the initial ratio indicating nitrogen-rich OM was preferentially consumed and phosphorus-rich OM being left behind. Overall, the initial C:N and C:P ratios were elevated and N:P ratio was lower when compared to the expected Redfield ratio for the FIPOM treatment in 2020, indicating carbon-rich, nitrogen-poor OM was present at in situ conditions, similar to the 2019 experiment.

As PON and POP were consumed, nitrate and phosphate concentrations should increase. In both 2019 and 2020, FIPOM – NO_3^- that was originally produced was consumed at later time points. Letscher et al. (2015) documented nitrate consumption in similar experiments examining DOM consumption in the South Pacific Gyre. Petrie and Yeats (2000) measured nitrate concentrations of 2 μM in the western Gulf of Maine basin during midfall in the late 90's, which is 9 – 10 times greater than the initial FIPOM concentration for 2019 and 2020 (0.22 μM and 0.2 μM , respectively). Additionally, in 2020, the changes in FIPOM – NO_3^- and PO_4^{3-} were inversely related to the cell counts for both incubations. When the population increased, the concentrations decreased, and vice versa. Based on the stoichiometric ratios of both the in situ PON:POP and $\text{NO}_3^- : \text{PO}_4^{3-}$, the Gulf of Maine at the time of collection each year was nitrogen poor. Bacteria can be nitrogen and phosphorus limited and become competitors with phytoplankton for these essential nutrients (Wheeler and Kirchman, 1986; Azam and Smith, 1991; Zweifel et al., 1993; Azam et al., 1994), which may explain the observed nitrate consumption in these incubation experiments performed in the dark.

In 2019, more nitrogen-rich OM was preferentially consumed at both temperatures, likely a result from the in situ microbial community being nitrogen limited. Whereas in 2020, more nitrogen-rich OM was preferentially consumed at cooler temperatures, leaving behind carbon-rich

OM, while at warmer temperatures, carbon-rich OM was preferentially consumed. This differential response of the C:N quality of OM consumed between temperatures in 2020 suggests C-rich OM may preferentially serve as the fuel sustaining elevated marine microbe metabolic rates at elevated temperatures. The initial OM in 2020 had an elemental stoichiometry of 494 C: 11.49 N: 1 P, very carbon-rich and nutrient-poor as compared to Redfield stoichiometry of average marine plankton. Biddanda and Benner (1997) found the marine phytoplankton in the Gulf of Mexico produced POM with a C:N ratio of 9 – 10 which is greater than the expected Redfield ratio and Goldman et al. (1979) observed marine diatoms to have a C:N ratio of 17 in stationary cultures. These values are still less than the values of the initial POM of 20 C: 1 N and 43 C: 1 N, for 2019 and 2020, respectively. Elevated C:P and N:P ratios in open ocean plankton biomass are associated with high temperature, lower nutrients, and less diversity of biomass (O'Reilly & Busch, 1984; Martiny et al., 2013; Martiny et al., 2016), environmental conditions that are typical during Fall in the Gulf of Maine (Thomas et al., 2003; Hu et al., 2011). Morán et al. (2020) showed that growth rates of tropical heterotrophic marine microbes were marginally affected from increasing temperatures, but the growth rates were more dependent on the elemental composition of the OM. The major differences between the OM stoichiometry from 2019 to 2020 [20 POC: 1 PON and 2 NO_3^- : 1 PO_4^{3-} for 2019 and 43 POC: 1 PON and 11.48 PON: 1 POP for 2020] could be due to the 2020 collection predating the Fall bloom by two weeks.

The estimated Q_{10} also exhibited variation, not the assumed canonical value of 2, between the elemental pools and years. In 2019, the consumption of POC was 26.6% faster and consumption of PON was 34.2% faster with a 1°C increase (a Q_{10} of 2 would predict a 20% increase for 1°C). Whereas in 2020, the overall consumption of PON was 12.1% faster, and the overall consumption of POP was 11.3% faster with a 1°C increase. This suggests temperature is

not the sole factor contributing to more rapid and a larger amount of marine OM consumed, but it plays an important role in marine OM consumption (this study; Lønborg et al., 2018). The stoichiometry of the OM and collection of OM regarding the timing of the phytoplankton bloom could be a major factor in the Q_{10} observed. Greater Q_{10} values in 2019 may be a result from the carbon-rich, very nitrogen-poor OM present and the marine microbes being in competition with other organisms for vital nutrients. On the other hand, the 2020 experiment had more carbon-rich OM and a larger quantity of nitrogen available for consumption, when compared to the 2019 experiment OM, and Q_{10} values exhibited less temperature sensitivity ($Q_{10} < 2$). Due to predating the phytoplankton bloom, marine microbes competing with phytoplankton for vital nutrients may not have been as intense. In addition to the composition of the OM, a shift in the community composition could explain the differences between the two years and is an area for future investigation. Due to the COVID – 19 shutdown, seasonal variability was not investigated, however, it cannot be ignored. Martiny et al. (2016) found seasonal variability in POM composition, ratios, and nutrient concentrations at the time series station Microbes in the Coastal Region of Orange County (MICRO) at Newport Pier off the coast of Southern California. Comparing the Fall bloom in the Gulf of Maine to the Spring bloom for POM composition, consumption rate and overall quantity between temperatures, nutrient concentrations, and community composition would be important to understand the temporal and annual variability, and to predict the potential impacts from climate change.

Warming ocean waters will increase and intensify stratification, reduce nutrient supply to the euphotic zone, creating more oligotrophic waters, and reduce gas solubility. Due to increasing metabolic rates with temperature, microbes will consume and remineralize more OM, weakening the biological pump while also leaving less OM to sink to the benthic ecosystems. Nearshore

benthic scavengers, such as lobsters, that rely on OM from the surface ocean may be negatively impacted as their food source will reduce, risking the marine food chain to collapse. Initial predictions for the empirically estimated temperature sensitivity of marine heterotrophic OM consumption yielded a Q_{10} value of 2.1 with a lower Q_{10} value of 1.5 for autotrophic primary production (Lopez-Urrutria et al., 2006), leading to predictions that the future metabolic balance of the marine ecosystem may eventually tip from its current state of net autotrophic (sink of atmospheric CO_2) to net heterotrophic (source of atmospheric CO_2) as marine respiration rates increase at a faster rate per unit temperature change. Our results found the Q_{10} of heterotrophic OM consumption to be between ~ 0.6 (inverse temperature effect) to ~ 3.4 which varied across years, weekly timescale events, and elemental pools. This suggests Q_{10} predictions may require further nuance including careful consideration of OM quality (carbon-rich or nutrient-rich), nutrient limitation status, regional, and interannual variability before application of Q_{10} or similar temperature sensitivity parameterizations of marine metabolic rates are included in Earth System Models, for example. Resolving the variability of marine respiration in relation to primary production Q_{10} values is an important, yet unrealized goal. If microbial consumption is indeed faster than primary production with increasing temperatures, more areas of CO_2 outgassing will likely appear across the ocean surface and reduce the amount of carbon sequestered to the deep ocean through sinking POM and yield an ineffective biological carbon pump. With the expansion of oligotrophic areas and faster consumption of marine POM, DOM export which dominates these regions (Letscher & Moore, 2017; Roshan & DeVries, 2017), may become more important for carbon sequestration in the biological carbon pump.

REFERENCES

- Allredge, A. L., and Silver, M. W., 1988, Characteristics, dynamics and significance of marine snow. *Progress in Oceanography*, v. 20, p. 41 – 82.
- Azam, F., and Smith, D. C., 1991, Bacterial Influence on the Variability in the Ocean's Biogeochemical State: A Mechanistic View. In: Demers S. (eds) *Particle Analysis in Oceanography*. NATO ASI Series (Series G: Ecological Sciences), v. 27, p. 213 – 236.
- Azam, F., Smith, D. C., Steward, G. F., and Hagström, 1994, Bacteria – Organic Matter Coupling and Its Significance for Oceanic Carbon Cycling. *Microbial Ecology*, v. 23, p. 167 – 179.
- Biddanda, B., and Benner, R., 1997, Carbon, nitrogen, and carbohydrate fluxes during the production of particulate and dissolved organic matter by marine phytoplankton. *Limnology and Oceanography*, v. 42(3), p. 506 – 518.
- Braman, R. S., and Hendrix, S.A., 1989, Nanogram Nitrite and Nitrate Determination in Environmental and Biological Materials by Vanadium (III) Reduction with Chemiluminescence Detection. *Analytical Chemistry*, v. 61, p. 2715 – 2718.
- Brewer, P. G., and Peltzer, E. T., 2017, Depth perception: the need to report ocean biogeochemical rates as functions of temperature, not depth. *Philosophical Transactions Royal Society*, v. 375, p. 1 – 18.
- Brown, J. H., Gillooly, J. F., Allen, A. P., Savage, V. M., and West, G. B., 2004, Toward a metabolic theory of ecology. *Ecology*, v. 85(7), p. 1771 – 1789.
- Durbin, E. G., Campbell, R. G., Casas, M. C., Ohman, M. D., Niehoff, B., Runge, J., and Wagner, M., 2003, Interannual variation in phytoplankton blooms and zooplankton productivity and abundance in the Gulf of Maine during winter. *Marine Ecology Progress Series*, v. 254, p. 81 – 100.
- Feldman, G. C., 2021, OceanColor WEB, NASA <https://oceancolor.gsfc.nasa.gov>
- Goldman, J. C., McCarthy, J. J., and Peavey, D. G., 1979, Growth rate influence on the chemical composition of phytoplankton in oceanic waters. *Nature*, v. 279, p. 210 – 215.
- Gran, H. H., and Braarud, T., 1935, A quantitative study of the phytoplankton in the Bay of Fundy and the Gulf of Maine (including observations on hydrography, chemistry and turbidity). *Journal of the Biological Board of Canada*, v. 1(5), p. 279 – 467.
- Hu, S., Chen, C., Ji, R., Townsend, D. W., Tian, R., Beardsley, R. C., and Davis, C. S., 2011, Effects of surface forcing on interannual variability of the fall phytoplankton bloom in the Gulf of Maine revealed using a process-oriented model. *Marine Ecology Progress Series*, v. 427, p. 29 – 49.

- Kamiya, E., Izumiyama, S., Nishimura, M., Mitchell, J. G., and Kogure, K., 2007, Effects of Fixation and Storage on Flow Cytometric Analysis of Marine Bacteria. *Journal of Oceanography*, v. 63, p. 101 – 112.
- Kirschbaum, M. U. F., 1995, The temperature dependence of soil organic matter decomposition, and the effect of global warming on soil organic storage. *Soil Biology and Biochemistry*, v. 27(6), p.753 – 760.
- Letscher, R. T., Knapp, A. N., James, A. K., Carlson, C. A., Santoro, A. E., and Hansell, D. A., 2015, Microbial community composition and nitrogen availability influence DOC remineralization in the South Pacific Gyre. *Marine Chemistry*, v. 177, p. 325 – 334.
- Letscher, R. T., and Moore, J. K., 2017, Modest net autotrophy in the oligotrophic ocean. *Biogeochemical Cycles*, v. 31(4), p. 699 – 708.
- Lønborg, C., Álvarez-Salgado, X. A., Letscher, R. T., and Hansell, D. A., 2018, Large Stimulation of Recalcitrant Dissolved Organic Carbon Degradation by Increasing Ocean Temperatures. *Frontiers in Marine Science*, v. 4, p. 1 – 11.
- López-Urrutia, A., San Martín, E., Harris, R. P., and Irigoien, X., 2006, Scaling the metabolic balance of the oceans. *PNAS*, v. 103, p. 8739 – 8744.
- Martiny, A. C., Vrugt, J. A., Primeau, F. W., and Lomas, M. W., 2013, Regional variation in the particulate organic carbon to nitrogen ratio in the surface ocean. *Global Biogeochemical Cycles*, v. 27, p. 723 – 731.
- Martiny, A. C., Pham, C. T. A., Primeau, F. W., Vrugt, J. A., Moore, J. K., Levin, S. A., and Lomas, M. W., 2013, Strong latitudinal patterns in the elemental ratios of marine plankton and organic matter. *Nature Geoscience*, v. 6, p. 279 – 283.
- Martiny, A. C., Talarmin, A., Mouginot, C., Lee, J. A., Huang, J. S., Gellene, A. G., and Caron, D. A., 2016, Biogeochemical interactions control a temporal succession in the elemental composition of marine communities. *Limnology and Oceanography*, v. 61, p. 531 – 542
- Morán, X. A. G., Calvo-Díaz, A., Arandia-Gorostidi, N., and Huete-Stauffer, T. M., 2018, Temperature sensitivities of microbial plankton net growth rates are seasonally coherent and linked to nutrient availability. *Environmental Microbiology*, v. 20, p. 3796 – 3810.
- O'Reilly, J. E., and Busch, D. A., 1984, Phytoplankton primary production on the northwestern Atlantic shelf. *Rapports et Proces-verbaux des Réunions. Conseil International pour l'Exploration de la Mer*, v. 183, p. 255 – 268.
- Pershing, A. J., Alexander, M. A., Hernandez, C. M., Kerr, L. A., Le Bris, A., Mills, K. E., Nye, J. A., Record, N. R., Scannell, H. A., Scott, J. D., Sherwood, G. D., and Thomas, A. C., 2015, Slow adaptation in the face of rapid warming leads to collapse of the Gulf of Maine cod fishery. *Science*, v. 350, p. 809 – 812.

- Petrie, B., and Yeats, P., 2000, Annual and interannual variability of nutrients and their estimated fluxes in the Scotian Shelf – Gulf of Maine region. *Canadian Journal of Fisheries and Aquatic Sciences*, v. 57(12), p. 2536 – 2546.
- Passow, U., 2002, Transparent exopolymer particles (TEP) in aquatic environments. *Progress in Oceanography*, v. 55, p. 287 – 333.
- Pomeroy, L. R., and Wiebe, W. J., 2001, Temperature and substrates as interactive limiting factors for marine heterotrophic bacteria. *Aquatic Microbial Ecology*, v. 23, p. 187 – 204.
- Redfield, A. C., 1934, On the proportions of organic derivatives in sea water and their relation to the composition of plankton. *James Johnstone Memorial Volume*, Liverpool, p. 177 – 192.
- Redfield, A. C., 1958, The biological control of chemical factors in the environment. *American Scientist*, v. 46(3), p. 205 – 221.
- Regaudie-de-Gioux, A., and Duarte, C. M., 2012, Temperature dependence of planktonic metabolism in the ocean. *Global Biogeochemical Cycles*, v. 26(GB1015), p. 1 – 10.
- Rivkin, R. B., and Legendre, L., 2001, Biogenic carbon cycling in the upper ocean: effects of microbial respiration. *Science*, v. 291, p. 2398 – 2400.
- Roshan, S., and DeVries, T., 2017, Efficient dissolved organic carbon production and export in the oligotrophic ocean. *Nature Communications*, v. 8(1), p. 1 – 8.
- Rosby, T., and Benway, R. L., 2000, Slow variations in mean path of the Gulf Stream east of Cape Hatteras. *Geophysical Research Letters*, v. 27, p. 117 – 120.
- Schneider, B., Schlitzer, R., Fischer, G., and Nöthig, E. M., 2003, Depth-dependent elemental compositions of particulate organic matter (POM) in the ocean. *Global Biogeochemical Cycles*, v. 17(2), p. 1 – 16.
- Sigler, M. F., Stabeno, P. J., Eisner, L. B., Napp, J. M., Mueter, F. J., 2014, Spring and fall phytoplankton blooms in a productive subarctic ecosystem, the eastern Bering Sea, during 1995 – 2011. *Deep Sea Research Part II*, v. 109, pg. 71 – 83.
- Solórzano, L., and Sharp, J. H., 1980, Determination of total dissolved phosphorus and particulate phosphorus in natural waters. *Limnology and Oceanography*, v. 25(4), p. 754 – 758.
- Strickland, J. D. H., and Parsons, T. R., 1968, Determination of reactive phosphorus. In: *A Practical Handbook of Seawater Analysis*. Fisheries Research Board of Canada, Bulletin 167, p. 49 – 56.
- Townsend, D. W., and Spinrad, R. W., 1986, Early spring phytoplankton blooms in the Gulf of Maine. *Continental Shelf Research*, v. 6(4), p. 515 – 529.

- Thomas, A. C., Townsend, D. W., and Weatherbee, R., 2003, Satellite-measured phytoplankton variability in the Gulf of Maine. *Continental Shelf Research*, v. 23(10), p. 971 – 989.
- Trombetta, T., Vidussi, F., Mas, S., Parin, D., Simier, M., and Mostajir, B., 2019, Water temperature drives phytoplankton blooms in coastal waters. *PLoS ONE*, v. 14, p. 1 – 28.
- Wheeler, P. A., and Kirchman, D. L., 1986, Utilization of inorganic and organic nitrogen by bacteria in marine systems. *Limnology and Oceanography*, v. 31, p. 998 – 1009.
- Yvon-Durocher, G., Schaum, C. E., and Trimmer, M., 2016, The Temperature Dependence of Phytoplankton Stoichiometry: Investigating the Roles of Species Sorting and Local Adaptation. *Frontiers in Microbiology*, v. 8, p. 1 – 14.
- Zhou, T., Shi, P., Hui, D., and Luo, Y., 2009, Global pattern of temperature sensitivity of soil heterotrophic respiration (Q_{10}) and its implication for carbon – climate feedback. *Journal of Geophysical Research: Biogeosciences*, v. 114(G2), p. 1 – 9.
- Zweifel, U. L., Norrman, B., and Hagström, Å., 1993, Consumption of dissolved organic carbon by marine bacteria and demand for inorganic nutrients. *Marine Ecology Progress Series*, v. 101, p. 23 – 32.